A free fermions in disguise model with claws

Kohei Fukai[1⋆], István Vona[2,3†] and Balázs Pozsgay[2‡]

1 Department of Physics, Graduate School of Science,
The University of Tokyo,
7-3-1, Hongo, Bunkyo-ku, Tokyo, 113-0033, Japan
2 MTA-ELTE "Momentum" Integrable Quantum Dynamics Research Group,
ELTE Eötvös Loránd University,
Pázmány P. sétány 1/A, H-1117 Budapest, Hungary
3 Holographic Quantum Field Theory Research Group,
HUN-REN Wigner Research Centre for Physics, Budapest, Hungary
⋆ kohei.fukai@phys.s.u-tokyo.ac.jp, † vona.istvan@wigner.hun-ren.hu, ‡ pozsgay.balazs@ttk.elte.hu

October 23, 2025

Abstract

Recently, several spin chain models have been discovered that admit solutions in terms of "free fermions in disguise." A graph-theoretical treatment of such models was also established, giving sufficient conditions for free fermionic solvability. These conditions involve a particular property of the so-called frustration graph of the Hamiltonian, namely that it must be claw-free. Additionally, one set of sufficient conditions also requires the absence of so-called even holes. In this paper, we present a model with disguised free fermions where the frustration graph contains both claws and even holes. Special relations between coupling constants ensure that the free fermionic property still holds. The transfer matrix of this model can be factorized in a special case, thereby proving the conjectured free fermionic nature of a special quantum circuit published recently by two of the present authors. This is the first example of free fermions in disguise with both claws and even holes simultaneously.

Contents

1 Introduction

The quest for exactly solvable quantum many-body systems has driven much of the progress in theoretical physics. Among the most tractable classes are systems mappable to free fermions, where the absence of interactions permits exact computation of many physical observables. The Jordan-Wigner transformation [1] stands as the archetypal example, converting local spin variables into fermionic operators and rendering numerous spin chain models exactly solvable [2,3].

Recent advances have expanded our understanding of free fermionic solvability beyond the traditional Jordan-Wigner paradigm. In [4] , Fendley discovered the "free fermions in disguise" (FFD) model, a spin chain that appears to have genuine four-fermion interactions, yet possesses hidden free fermionic structures. The model exhibits the remarkable property of remaining free fermionic for arbitrary coupling constants, including fully disordered configurations.

Subsequently, graph-theoretical frameworks were established to characterize free fermionic solvability systematically. Two independent works [5] and [6] first derived graph-theoretical criteria for generalized Jordan-Wigner transformations. Afterwards, a comprehensive framework was established in [7, 8], which unified both Jordan-Wigner and FFD models. Extensions to parafermionic commutation relations were treated in [9–11].

Importantly, the papers [7, 8] derived sufficient conditions for free fermionic solvability that apply for all possible choices of the coupling constants. However, these conditions are not necessary, as the original works themselves noted [7,8]. This leaves room for models that do not satisfy all of these conditions, while maintaining free fermionic structures through special selections of the coupling constants. One of the sufficient conditions is the so-called "claw-free" property of the frustration graph. A concrete example of a free fermionic model violating this condition was given in [12], which achieved solvability through a particular extension of the FFD algebra.

In this work, we present another example of a free fermionic model "with claws". Most notably, our model also contains "even holes", which pose additional algebraic challenges for constructing free fermionic solutions [8]. This is the first example of a disguised free fermion model that exhibits both claws and even holes simultaneously. The model Hamiltonian was inspired by the recent work [13] of two of the present authors, where selected quantum circuits were conjectured to have free fermionic solvability. We prove one of these conjectures by showing that the transfer matrix of our current model becomes proportional to the quantum circuit in question for a special choice of the spectral parameter.

The solvability is achieved through carefully constructed algebraic relations among the coupling constants that compensate for the graph-theoretical obstructions. We derive these relations through introducing an extension of the FFD algebra with imposed algebraic conditions. Our Hamiltonian can also be formulated solely within the original FFD algebra for a special case, unlike [12]. We successfully solve the inverse problem by expressing local operators in terms of free fermionic modes, following the methodology of [14]. We further compute real-time correlation functions for selected operators. The number of fermionic eigenmodes in our model is the same as in the original FFD model, resulting in an exponentially large symmetry algebra analogous to that recently characterized for the FFD case in [15].

The structure of this paper is as follows. In Sec. 2, we review previous progress on the FFD and introduce a new free fermionic Hamiltonian. In Sec. 3, we propose an extension of the FFD algebra and derive the new Hamiltonian from this extended algebra. In Sec. 4, we provide a family of commuting conserved charges. We introduce the transfer matrix in Sec. 5 and the fermionic eigenmodes in Sec. 6. In Sec. 7, we solve the inverse problem and compute correlation functions. In Sec. 8, we discuss the factorization of the transfer matrix, and finally in Sec. 9, we present our conclusions. Certain technical parts of the proofs are presented in the Appendices.

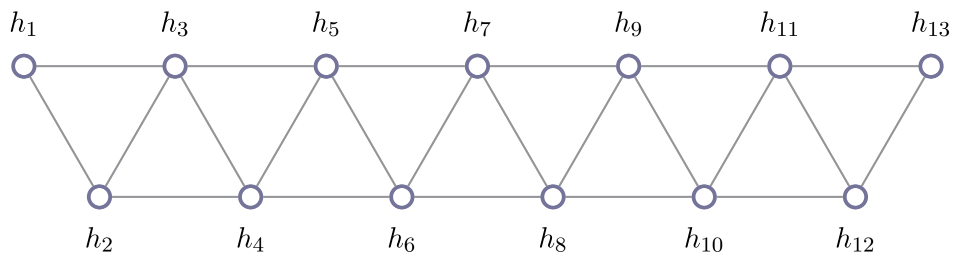

Figure 1: Frustration graph for the original FFD model ($M = 13$ case). Each vertex represents a generator of the FFD algebra. Vertices are connected by an edge when the corresponding generators anticommute.

2 The FFD algebra

In this section, we first review the graph-theoretical framework of the FFD model [7] and then introduce our spin chain Hamiltonian, explaining how it extends the original Hamiltonian of [4] . In later sections, we present the frustration graph for our FFD Hamiltonian, which contains both claws and even holes, and prove that the Hamiltonian is integrable and can be solved using free fermionic operators.

2.1 Review of the FFD algebra

We first review the algebra introduced by Fendley in [4] , which we dub FFD algebra. This algebra is made of the generators $\{h_j\}_{j=1}^{M}$, where $M \geq 1$ is some integer. The square of the generators are scalars[1]:

$$h_m^2 = b_m^2\,, \tag{1}$$

where b_m are arbitrary coupling constants. The generators are anticommuting when the indices are neighboring or next to neighboring, and commuting otherwise:

$$\begin{aligned} h_m h_{m+1} &= -h_{m+1} h_m & (2)\\ h_m h_{m+2} &= -h_{m+2} h_m & (3)\\ h_m h_l &= h_l h_m \quad (|l-m| > 2)\,. & (4) \end{aligned}$$

There is no periodicity condition for the indices, therefore the algebra naturally describes models with open boundary conditions. The FFD algebra is a particular case of a generalized Clifford algebras.

The standard presentation of the FFD algebra can be given for a spin-1/2 chain as follows. Let the Pauli matrix acting on the j-th site be denoted by σ_j^α, where $\alpha \in \{x, y, z\}$ indicates the component of the Pauli matrix. Then we have

$$h_m = b_m \sigma_m^z \sigma_{m+1}^z \sigma_{m+2}^x. \tag{5}$$

For other presentations, see [4, 13].

The original FFD Hamiltonian of Fendley [4] reads simply

$$H_{\text{FFD}} = \sum_{m=1}^{M} h_m, \tag{6}$$

[1]Some of the previous work on the topic used a different convention, namely to have $h_m^2 = 1$ and to add the coupling constants separately to the Hamiltonian.

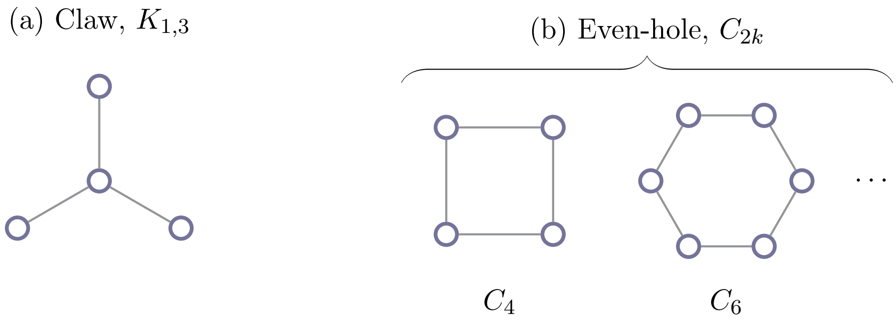

Figure 2: Forbidden structures in a frustration graph for free fermionic solutions of [7]: (a) the claw $K_{1,3}$ and (b) an even hole C_{2k}. A graph is claw-free or even-hole-free if none of its induced subgraphs contain a claw or an even hole. The frustration graph in Figure 1 is (even-hole, claw)-free.

where the Hamiltonian is comprised of the sum of all FFD generators. The higher-order charges are constructed from products of FFD generators [4] .

We next explain the frustration graph. Generally, the frustration graph is defined for spin chain Hamiltonians where the individual terms either commute or anticommute, and this condition is fulfilled if the Hamiltonian is expressed as a sum of products of Pauli matrices. Each term in the Hamiltonian corresponds to a vertex in the graph, and two vertices are connected if and only if the two terms in question anticommute. For an extension to the more general case of parafermionic commutation relations, see [11, 16].

The frustration graph for the FFD algebra is shown in Figure 1. This graph has the property of being *(even-hole, claw)-free* [7]. The structures of even holes and the claw are illustrated in Figure 2. The seminal result in [7] is that any Hamiltonian with a frustration graph that is (even-hole, claw)-free can be solved by free fermions in disguise [4] . Thus, we can solve the FFD Hamiltonian (6) using these methods.

In [8], the framework of (even-hole, claw)-free are generalized to *simplicial, claw-free*, which also admit the existence of even holes in the frustration graph. However, there is no example still now that the disguised free fermion model with both claw and even hole.

In the following, we present a model with free fermions in disguise that have both claws and even holes for the first time.

2.2 An extended FFD Hamiltonian

We propose a new integrable Hamiltonian in terms of the FFD algebra:

$$H_M = \sum_{m=1}^{M} h_m + \sum_{m=2}^{\lfloor M/2 \rfloor} \beta_{2m-1} h_{2m-2} h_{2m-3} h_{2m} \,, \tag{7}$$

where $\{\beta_3, \beta_5, \beta_7, \ldots\}$ are additional coupling constants that satisfy the relations

$$\beta_{2m+1} = \frac{\beta_{2m-1}}{b_{2m-4}^2 \beta_{2m-3} - b_{2m}^2 \beta_{2m-1} + 1} \quad (m > 2) \,. \tag{8}$$

We started the index of the additional coupling from β_3 because of the later use. The initial values for the recursion, β_3 and β_5 can be chosen arbitrarily. The ordering of the triple product in (7) is adopted for the purpose of simplification presented below.

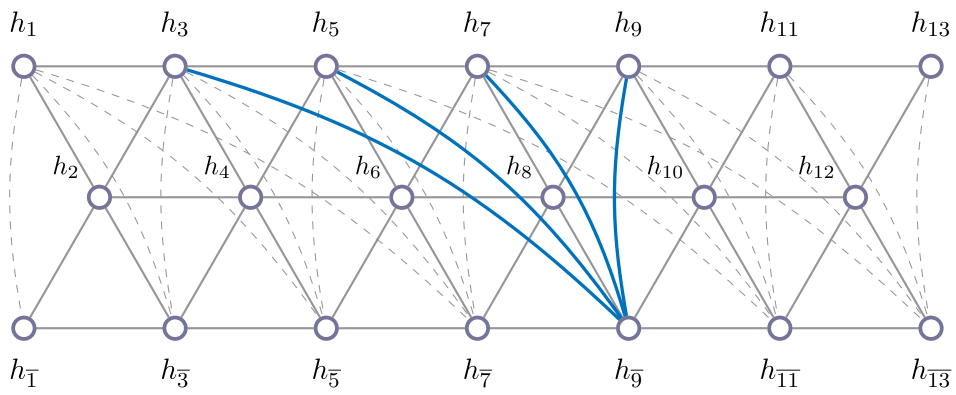

Figure 3: Frustration graph for the extended FFD algebra $G_{M=13}$. Vertices are connected by an edge when the corresponding generators anticommute. The edges between $\{h_m\}$ and $\{h_{\overline{m'}}\}$ are represented by dotted lines. To highlight the basic structure, we have highlighted the dotted edges from $h_{\overline{9}}$ with solid blue lines. The other dotted lines are obtained by translation.

The new model (7) can be seen as a deformation of the original FFD model [4] . The first term in (7) is equal to the Hamiltonian of the original FFD model, and the second term is the new interaction term, which retains the free fermionic solvability. The original FFD Hamiltonian (6) is reproduced in the limit $\beta_{2m-1} \equiv 0$.

In the next section, we will show the frustration graph for the Hamiltonian (7) and demonstrate that it contains both claws and even holes. We will also derive this new integrable Hamiltonian from an algebraic extension of the original FFD algebra.

3 The extended FFD algebra

In this section, we introduce an algebraic extension of the FFD algebra. We first introduce additional generators and the frustration graph for the extended algebra. Then we impose an algebraic relation on them, which ensures free-fermionic integrability, and show the generalized integrable Hamiltonian. Finally, we reproduce the new Hamiltonian (7) as a special case. We consider the case where the number of generators of the original FFD algebra is odd: $M = 2M' + 1$. However, our argument can be extended to the even M case with $M = 2M'$.

3.1 Additional generators and the frustration graph

We propose an algebraic extension of the FFD algebra with new generators $\{h_{\overline{2m+1}}\}_{m=0}^{M'}$. As in the original FFD algebra, the squares are scalars:

$$h_{\overline{2m-1}}^2 = b_{\overline{2m-1}}^2, \tag{9}$$

where $b_{\overline{2m-1}}$ is a coupling constant. The generator $h_{\overline{2m-1}}$ anticommutes with the following FFD generators with odd indices:

$$\{h_{\overline{2m-1}}, h_{2m-7}\} = \{h_{\overline{2m-1}}, h_{2m-5}\} = \{h_{\overline{2m-1}}, h_{2m-3}\} = \{h_{\overline{2m-1}}, h_{2m-1}\} = 0, \tag{10}$$

and also with those with even indices:

$$\{h_{\overline{2m-1}}, h_{2m-2}\} = \{h_{\overline{2m-1}}, h_{2m}\} = 0, \tag{11}$$

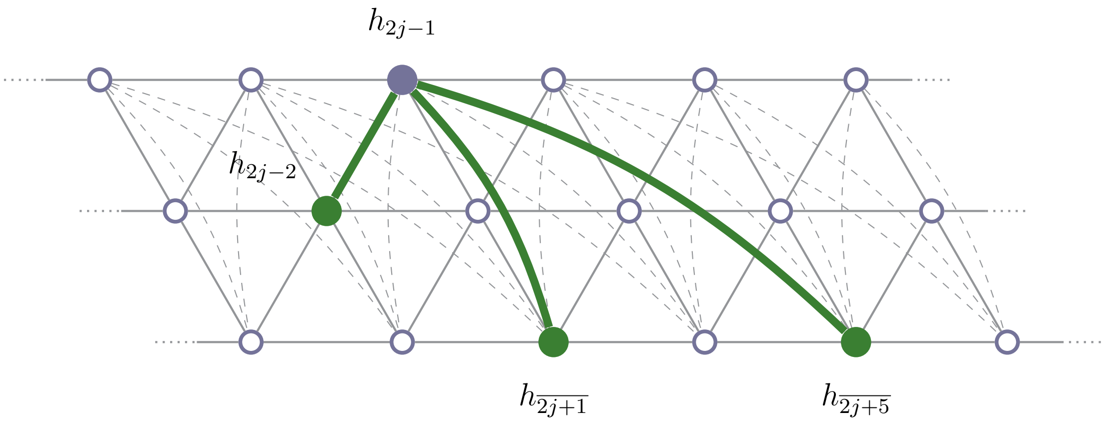

(a) Type A claw at h_{2j-1}

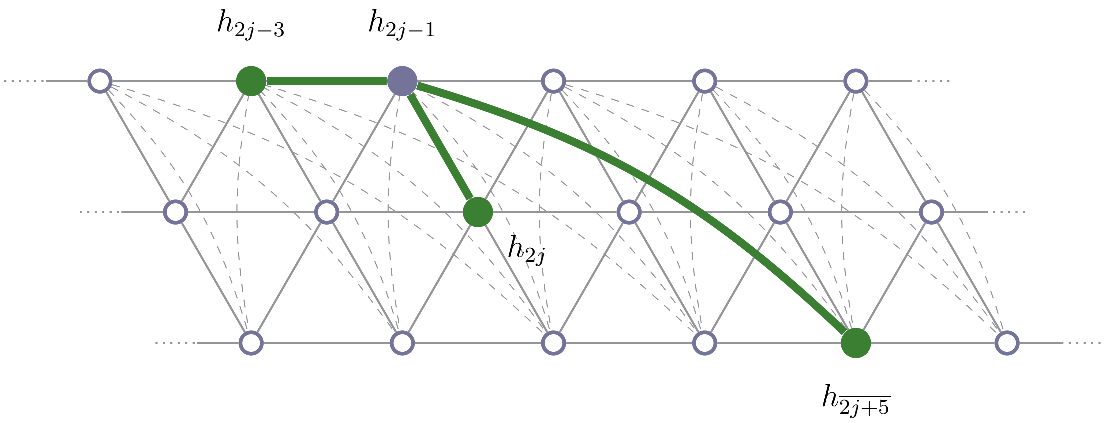

(b) Type B claw at h_{2j-1}

Figure 4: Structures of claws centered at h_{2j-1}. The bold green edges connect the claw center (grayish-blue circle) to its three leaves (green circles), while gray edges indicate all other edges in the frustration graph. (a) Type A claw: leaves are located at vertices h_{2j-2}, $h_{\overline{2j+1}}$, and $h_{\overline{2j+5}}$. (b) Type B claw: leaves are located at vertices h_{2j-3}, h_{2j}, and $h_{\overline{2j+5}}$. Note that both claw types share the common leaf $h_{\overline{2j+5}}$. For a more detailed structural analysis, see Figure 9.

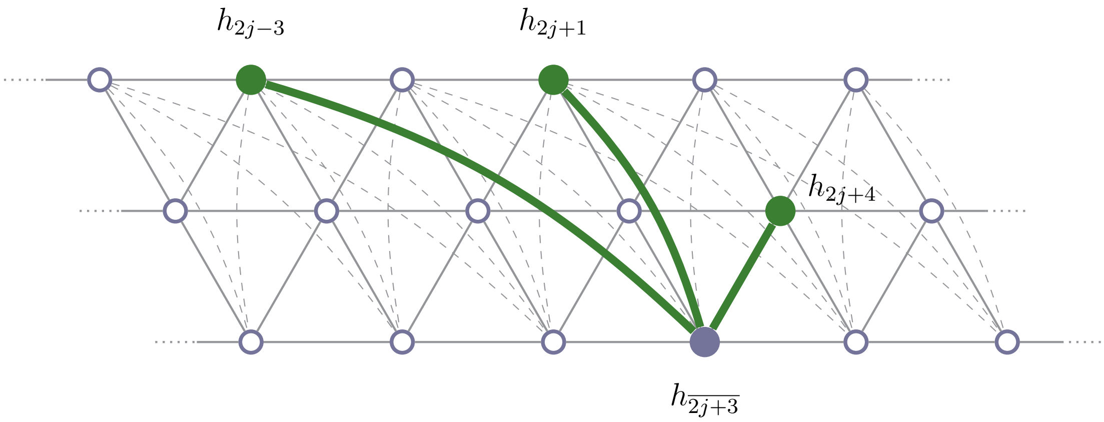

(a) Type A claw at $h_{\overline{2j+3}}$

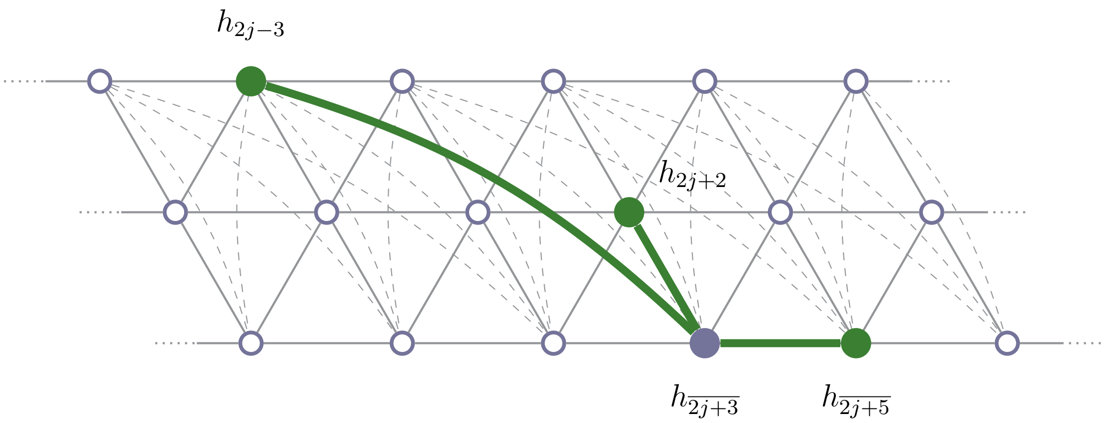

(b) Type B claw at $h_{\overline{2j+3}}$

Figure 5: Structures of claws centered at $h_{\overline{2j+3}}$. The bold green edges connect the claw center (grayish-blue circle) to its three leaves (green circles), while gray edges indicate all other edges in the frustration graph. (a) Type A claw: leaves are located at vertices h_{2j-3}, h_{2j+1}, and h_{2j+4}. (b) Type B claw: leaves are located at vertices h_{2j-3}, h_{2j+2}, and $h_{\overline{2j+5}}$. Note that both claw types share the common leaf h_{2j-3}. For a more detailed structural analysis, see Figure 10.

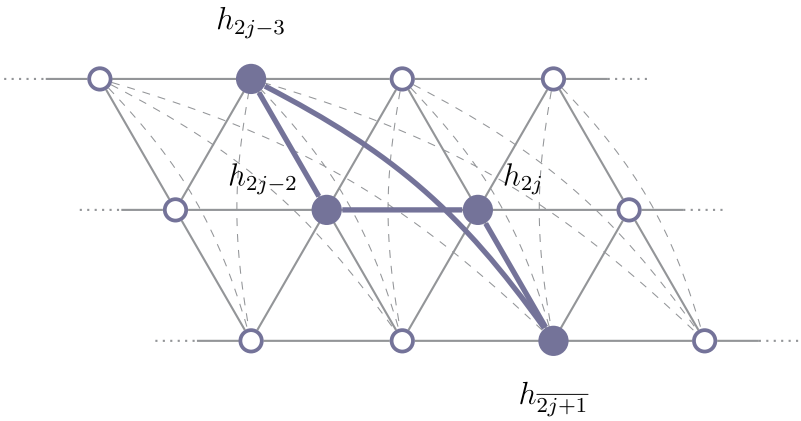

Figure 6: Structure of an even hole C_4 in the frustration graph for the extended FFD algebra: $\mu_{2j-1} = h_{2j-3}h_{2j}h_{2j-2}h_{\overline{2j+1}}$. The vertices in the even hole are represented by blue-filled circles and the four edges in the even hole are represented by bold blue lines.

as well as within the extended algebra:

$$\{h_{\overline{2m-1}}, h_{\overline{2m+1}}\} = 0, \tag{12}$$

and commutes with all others.

Following [7,8] we introduce the frustration graph for the extended FFD algebra. We show the frustration graph G_M for this extended FFD algebra in Figure 3, where the additional vertices for $h_{\overline{2j-1}}$ are placed in the lower row, and the dotted edges represent the anticommutation relations (10).

3.2 Claw in the extended frustration graph

A notable property of the new frustration graph is that it contains claws. We show the claws in the frustration graph for the extended FFD algebra in Figures 4 and 5. The claw center can be h_{2j-1} or $h_{\overline{2j-1}}$, with leaves shown in Figure 4 for claws centered at h_{2j-1} and in Figure 5 for those centered at $h_{\overline{2j-1}}$. Hereafter, we refer to a claw with center h_c as a "claw at h_c".

Claws with the same center have two patterns: type A and type B. Let the three leaves of a claw at center h_c be denoted by $\mathcal{L}_c^t = (h_c^{\mathcal{L},t,1}, h_c^{\mathcal{L},t,2}, h_c^{\mathcal{L},t,3})$. For claws at h_{2j-1} (Figure 4): type A has leaves at the vertices $\mathcal{L}^A_{2j-1} \equiv (h_{\overline{2j+1}}, h_{2j-2}, h_{\overline{2j+5}})$, while type B has leaves at the vertices $\mathcal{L}^B_{2j-1} \equiv (h_{2j-3}, h_{2j}, h_{\overline{2j+5}})$. For claws at $h_{\overline{2j+3}}$ (Figure 5): type A has leaves at the vertices $\mathcal{L}^A_{\overline{2j+3}} \equiv (h_{2j+1}, h_{2j+4}, h_{2j-3})$, while type B has leaves at the vertices $\mathcal{L}^B_{\overline{2j+3}} \equiv (h_{\overline{2j+5}}, h_{2j+2}, h_{2j-3})$. Note that the leaf $h_c^{\mathcal{L},t,3}$ remains the same for both claw types with the same center c, and we denote $h_c^{\mathcal{L}} \equiv h_c^{\mathcal{L},t,3}$.

The range of claw centers is as follows: when h_c with $c = 2m-1$ is a claw center, then $3 \le c \le 2M' - 5$; when $h_{\overline{c}}$ is a claw center, then $7 \le c \le 2M' - 1$.

The sufficient conditions of [7,8] for integrability and free fermionic solvability include claw-freeness of the frustration graph. At first sight, having claws seems to imply that the methods of [7,8] cannot be applied. However, the situation is different. The works [7,8] treated models where the terms in the Hamiltonian were functionally independent from each other. In our case, this is not true because we have the relations (19). We will argue that these extra relations, supplied with (19), salvage the applicability of the results of [7,8].

3.3 Even hole in the extended frustration graph

Another notable point for the new frustration graph is that there exist even holes C_4. We show an even hole in the frustration graph for the extended FFD algebra in Figure 6. Even holes are formed by following four generators: $\{h_{2m-3}, h_{2m}, h_{2m-2}, h_{\overline{2m+1}}\}$ for $1 < m \leq M'$. We define μ_{2m-1} as the product of these generators:

$$\mu_{2m-1} \equiv h_{2m-3}h_{2m}h_{2m-2}h_{\overline{2m+1}} \quad \text{for } 1 < m \leq M'. \tag{13}$$

The important feature of (13) is that it is central in the extended FFD algebra; μ_{2m-1} commutes with all generators in the extended FFD algebra: $[\mu_{2m-1}, h_{m'}] = 0$ for $1 \leq m' \leq M$, and $[\mu_{2m-1}, h_{\overline{2m'+1}}] = 0$ for $0 \leq m' \leq M'$. These properties can be proven from the fact that each vertex in the frustration graph has zero, two, or four connections to the vertices in the even hole, as can be confirmed in Figure 6.

Moreover, its square is a scalar: $\mu_{2m-1}^2 = b_{2m-3}^2 b_{2m}^2 b_{2m-2}^2 b_{\overline{2m+1}}^2$. Thus, we can treat μ_{2m-1} as a scalar:

$$\mu_{2m-1} = \pm b_{2m}b_{2m-3}b_{2m-2}b_{\overline{2m+1}}\,, \tag{14}$$

where the sign factor is chosen for each central element μ_{2m-1}. Therefore, we can express the extra generator $h_{\overline{2m+1}}$ as

$$h_{\overline{2m+1}} = \beta_{2m-1}h_{2m-2}h_{2m-3}h_{2m} \quad \text{for } 1 < m \leq M', \tag{15}$$

where we define

$$\beta_{2m-1} \equiv \pm \frac{b_{\overline{2m+1}}}{b_{2m-2}b_{2m-3}b_{2m}}. \tag{16}$$

Here, we can see that the triple products in the new Hamiltonian (7) can be derived from the extended FFD algebra as in (15).

Note that $h_{\overline{1}}$ and $h_{\overline{3}}$ cannot be expressed in terms of the generators of the original FFD algebra.

One might wonder about the choice of sign for μ_{2m-1}; however, this choice is absorbed into the definition of $b_{\overline{2m+1}}$ because algebraically, only its square appears in the definition of the extended algebra. Different sign choices are absorbed into different sign choices for $b_{\overline{2m+1}}$ at the definitional level.

3.4 Extra relations for free fermionic integrability

We further impose relations among the generators of the extended algebra. We first define the following quantities:

$$\mathbb{A}_{2m-1} \equiv h_{2m}h_{2m-3} + h_{2m-2}h_{\overline{2m+1}}, \tag{17}$$

$$\mathbb{C}_{2m} \equiv h_{2m-3}h_{\overline{2m+3}}. \tag{18}$$

We then require the following relation between the generators:

$$\mathbb{A}_{2m-1}\mathbb{C}_{2m+2} = \mathbb{C}_{2m}\mathbb{A}_{2m+3} \quad \text{for } 1 < m < M' - 1. \tag{19}$$

Substituting (15) into (19), we obtain the relation (8):

$$\begin{aligned}\mathbb{A}_{2m-1}\mathbb{C}_{2m+2} - \mathbb{C}_{2m}\mathbb{A}_{2m+3} = {}& \left[\beta_{2m+1}(1+\beta_{2m+3}b_{2m+2}^2) - \beta_{2m+3}(1+\beta_{2m-1}b_{2m-2}^2)\right] \\ & \times h_{2m-3}h_{2m-1}h_{2m}h_{2m+2}h_{2m+1}h_{2m+4}\,, \end{aligned} \tag{20}$$

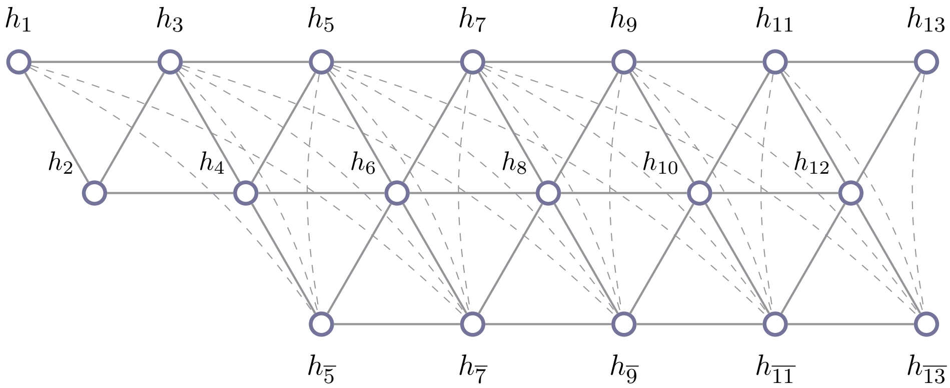

Figure 7: Frustration graph for the Hamiltonian (7) ($M = 13$). The vertices $h_{\overline{1}}$ and $h_{\overline{3}}$ are not present for this case.

thus we have

$$\beta_{2m+1}(1 + \beta_{2m+3} b_{2m+2}^2) = \beta_{2m+3}(1 + \beta_{2m-1} b_{2m-2}^2)\,, \tag{21}$$

which is equivalent to (8) with the index shift $m \to m-1$, except when $1+\beta_{2m-1}b_{2m-2}^2 - \beta_{2m+1}b_{2m}^2 = 0$. The latter case is not considered here.

The condition (19) does not constrain the following coupling constants: $b_{\overline{1}}$, $b_{\overline{3}}$, $b_{2M'-1}$, and $b_{2M'+1}$. Thus, we can choose these coupling constants freely.

Among the remaining couplings, they must satisfy (19). The number of remaining couplings is $4M' - 2$, and the number of constraints from (19) is $M' - 3$, yielding $3M' + 1$ free parameters among the remaining couplings. If we freely choose $\{b_m\}_{m=1}^{2M'+1}$ and set $b_{\overline{5}}$ and $b_{\overline{7}}$, then all other couplings $\{b_{\overline{2m+1}}\}_{m=4}^{M'}$ are determined by the relation (19), or equivalently by the recursion relations (8) and (16).

Since the coupling constants $b_{2M'-1}$ and $b_{2M'+1}$ can be set freely, we can set them to zero. Figure 8(a) shows the frustration graph G_{2m+1}. Setting $b_{2m+1} = 0$ (i.e., removing the vertex h_{2m+1}) yields the frustration graph $G_{2m} = G_{2m+1}\big|_{b_{2m+1}=0}$ for the Hamiltonian (7) with even $M = 2m$ (Figure 8(b)). Furthermore, removing the vertices h_{2m-1} and h_{2m+1} yields the frustration graph $G'_{2m} = G_{2m}\big|_{b_{2m-1}=0}$ shown in Figure 8(c). We call a frustration graph *free fermionic* if mutually commuting charges can be defined on it; in other words, if there is no contradiction with the relation (19). The frustration graphs in Figure 8 are free fermionic frustration graphs. For Figure 8(c), we can further eliminate the vertices h_{2m-3} and $h_{\overline{2m+1}}$ simultaneously, as depicted in Figure 18, which gives another free fermionic frustration graph.

For the left edge of the graph, corresponding to $b_{\overline{1}}$ and $b_{\overline{3}}$, the frustration graph for the free fermionic model must have the same structure as in Figure 8, but rotated by 180 degrees.

As we will see later, the relation (19) is crucial for the existence of higher-order charges of the Hamiltonian (7) and thus its integrability.

3.5 Representation of the extended FFD algebra

We now show the representation for the extended algebra. From (15), for $2 \le m \le M'$, $h_{\overline{2m+1}}$ can be represented using the representation of the original FFD algebra (5).

However, $h_{\overline{1}}$ and $h_{\overline{3}}$ cannot be represented by the original FFD representation (5). They

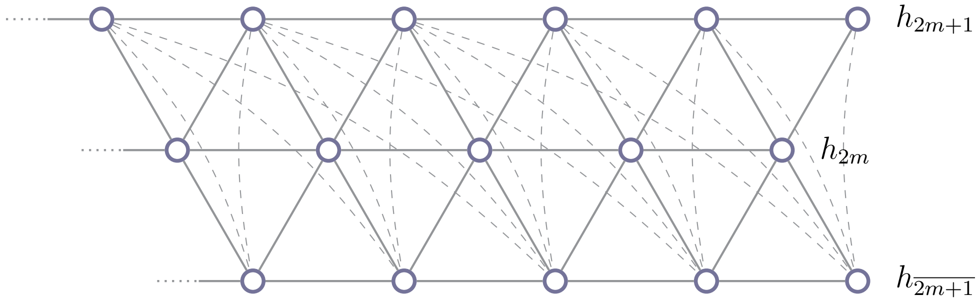

(a) Free fermionic frustration graph G_{2m+1}

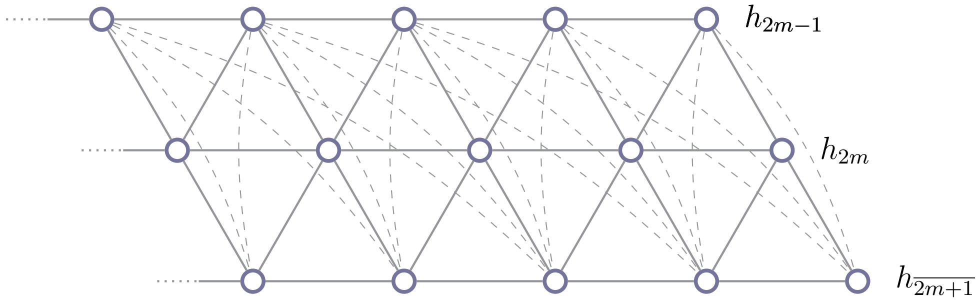

(b) Free fermionic frustration graph G_{2m}

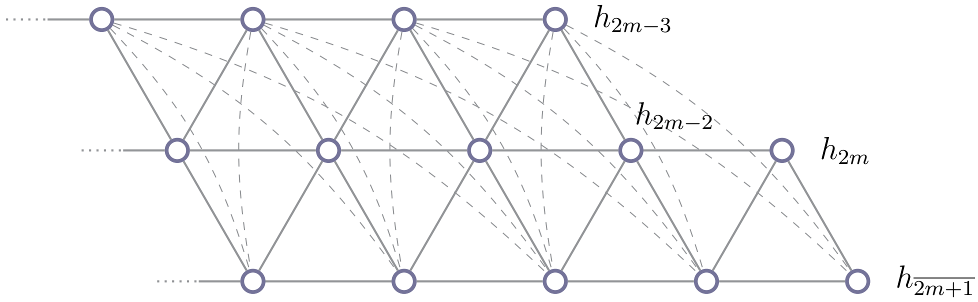

(c) Free fermionic frustration graph G'_{2m}

Figure 8: Free fermionic frustration graphs. (a) The frustration graph G_{2m+1}. (b) The frustration graph $G_{2m+1}|_{b_{2m+1}=0} = G_{2m}$. This frustration graph corresponds to the new Hamiltonian (7) with even M. (c) The frustration graph $G_{2m+1}\big|_{b_{2m+1},b_{2m-1}=0} = G'_{2m}$. The Hamiltonians corresponding to these frustration graphs can be proven to be free fermionic. The left edge of the frustration graph should also have these configurations rotated by 180 degrees.

require representations outside the original one (5):

$$h_{\overline{1}} = b_{\overline{1}}\sigma_1^z\sigma_2^y\,, \tag{22}$$

$$h_{\overline{3}} = b_{\overline{3}}\sigma_1^y\sigma_2^y\sigma_3^z\sigma_4^x\,. \tag{23}$$

3.6 General integrable Hamiltonian

We define the abstract Hamiltonian in terms of the extended FFD algebra:

$$H_M = \sum_{m=1}^{M} h_m + \sum_{m=0}^{\lfloor M/2\rfloor} h_{\overline{2m+1}}\,, \tag{24}$$

and the corresponding frustration graph is G_M. This Hamiltonian includes the previously introduced Hamiltonian (7) as a special case with coupling constants $b_{\overline{1}} = b_{\overline{3}} = 0$. Again, the Hamiltonian for even $M = 2M'$ can be obtained from $H_{2M'+1}\big|_{b_{2M'+1}=0}$, whose corresponding frustration graph is $G_{2M'}$.

In Section 4, we prove that the Hamiltonian (24) has an extensive number of mutually commuting charges. The condition (19) is crucial for the existence of these higher-order charges and their mutual commutativity. In Section 5, we introduce the transfer matrix for the model (24) and derive its recursion relation.

From Section 6 onward, we consider only the Hamiltonian with $b_{\overline{1}} = b_{\overline{3}} = 0$, i.e., the Hamiltonian (7), which can be constructed within the original FFD algebra. The frustration graph for the Hamiltonian (7) is shown in Figure 7. Nevertheless, the more general Hamiltonian (24) can also be solved in the same way.

4 Conserved charges

In this section, we give an extensive number of conserved charges for the Hamiltonian (24). We first introduce notations for a graph-theoretical description of the charges. Then we define the extensive number of charges and provide a proof of the conservation laws. In Appendix A, we provide the proof for the mutual commutativity of the charges.

4.1 Notations

We introduce the graph-theoretical notation used throughout this paper in a similar manner as in [7]. A graph $G = (V, E)$ consists of a finite vertex set V and an edge set $E \subseteq V^{\times 2}$, where each edge is a 2-element subset of V. All graphs considered are simple (no self-loops or multiple edges).

For any subset $S \subseteq V$, the induced subgraph is denoted by $G[S] = (S, E \cap S^{\times 2})$, which contains all vertices in S and all edges from E with both endpoints in S. We also define the shorthand notation $E_S \equiv E \cap S^{\times 2}$. Throughout this paper, we often refer to a subset of vertices interchangeably with the subgraph it induces.

The open neighborhood of a vertex v is $\Gamma(v) = \{u \in V \mid \{u, v\} \in E\}$, consisting of all vertices neighboring v. The closed neighborhood is $\Gamma[v] = \Gamma(v) \cup \{v\}$, which includes v itself.

An independent set of a graph $G = (V, E)$ is a subset of vertices $S \subseteq V$ which induces a subgraph with no edges, i.e., $G[S] = (S, \emptyset)$. Equivalently, S is independent if and only if no two vertices in S are adjacent.

A *clique* K in a graph $G = (V, E)$ is a subset of vertices such that every pair of vertices in K is neighboring.

Now we introduce the notation for the frustration graph of our model. First, we introduce the vertex set for the original FFD Hamiltonian (6): $V_M^{\mathrm{FFD}} \equiv \{1, 2, \ldots, M\}$, where each vertex corresponds to a term in the Hamiltonian (6), i.e., the vertex labeled as j denotes the FFD generator h_j. The original edge set of the FFD algebra is given by

$$E_M^{\mathrm{FFD}} \equiv \{(m, n) \in V_M^{\mathrm{FFD}} \times V_M^{\mathrm{FFD}} \mid \{h_m, h_n\} = 0\}. \tag{25}$$

We next introduce the additional vertices for the additional generators in the Hamiltonian (24): $\overline{V}_M \equiv \{\overline{1}, \overline{3}, \ldots, \overline{2\lfloor M/2 \rfloor + 1}\}$. Note that the indices with overlines consist of odd integers. Each vertex corresponds to a term in the Hamiltonian. The vertex labeled by an overlined index $\overline{2m+1}$ represents the extra generator $h_{\overline{2m+1}}$. We also define the union of these two sets as $V_M \equiv V_M^{\mathrm{FFD}} \cup \overline{V}_M$. We introduce the notation for the frustration graph of the extended FFD algebra $G_M = (V_M, E_M)$, where the set of edges is defined by

$$E_M \equiv \{(\boldsymbol{i}, \boldsymbol{j}) \in V_M \times V_M \mid \{h_{\boldsymbol{i}}, h_{\boldsymbol{j}}\} = 0\}, \tag{26}$$

which correspond to the edges in Figure 3. The frustration graph for the extend FFD algebra introduced previous section is $G_M = (V_M, E_M)$. With this notation, the Hamiltonian (24) is rewritten as

$$H_M = \sum_{\boldsymbol{j} \in V_M} h_{\boldsymbol{j}}. \tag{27}$$

In the following, we often identify the vertex $\boldsymbol{j} \in V_M$ with the corresponding generator $h_{\boldsymbol{j}}$.

4.2 Higher-order charges

In this subsection, we introduce the higher-order charges of the Hamiltonian (24) and prove their conservation law.

Let $\mathcal{S}_M^{(k)}$ denote the collection of all independent sets of order k in $G_M = (V_M, E_M)$. For $S \in \mathcal{S}_M^{(k)}$, any two generators from S mutually commute:

$$[h_{\boldsymbol{i}}, h_{\boldsymbol{j}}] = 0 \quad \text{for all } \boldsymbol{i}, \boldsymbol{j} \in S. \tag{28}$$

The charges are defined as sums of products of commuting generators:

$$Q_M^{(k)} \equiv \sum_{S \in \mathcal{S}_M^{(k)}} \prod_{\boldsymbol{i} \in S} h_{\boldsymbol{i}}. \tag{29}$$

Note that the first charge is the Hamiltonian itself: $Q_M^{(1)} = H_M$. The highest value for k is the independence number of the frustration graph, denoted by S_M, that is, the cardinality of its largest independent vertex set. For $k > S_M$, we have $Q_M^{(k)} = 0$. In our case, $S_M = \lfloor (M+2)/3 \rfloor$, similarly to the original FFD case, which can be seen from the recursion equations for the polynomials (49) and (50); the proof is given in Appendix D.

Theorem 1. *The charges defined in* (29) *are conserved:*

$$[H_M, Q_M^{(k)}] = 0 \qquad \forall k \in \{1, 2, \ldots, S_M\}. \tag{30}$$

Proof. The proof follows the strategy of Lemma 1 in [7]. For any independent set $S \subset V_M$, we define

$$h_S \equiv \prod_{\boldsymbol{j} \in S} h_{\boldsymbol{j}}. \tag{31}$$

For any $\boldsymbol{j} \in V_M$ and independent set $S \subset V_M$, we have

$$[h_{\boldsymbol{j}}, h_S] = \begin{cases} 2h_{\boldsymbol{j}} h_S & \text{if } |\Gamma(\boldsymbol{j}) \cap S| \text{ is odd,} \\ \\ 0 & \text{if } |\Gamma(\boldsymbol{j}) \cap S| \text{ is even.} \end{cases} \tag{32}$$

The commutator of the Hamiltonian with the charge is then

$$[H_M, Q_M^{(k)}] = 2 \sum_{\boldsymbol{j} \in V_M} \sum_{\substack{S \in \mathcal{S}_M^{(k)} \\ |\Gamma(\boldsymbol{j}) \cap S| = 1}} h_{\boldsymbol{j}} h_S + 2 \sum_{\boldsymbol{j} \in V_M} \sum_{\substack{S \in \mathcal{S}_M^{(k)} \\ |\Gamma(\boldsymbol{j}) \cap S| = 3}} h_{\boldsymbol{j}} h_S. \tag{33}$$

We show that both terms vanish separately.
Cancellation of the first term: This follows the same argument as in the original FFD case [4,7]. Consider $\boldsymbol{j} \in V_M$ and $S \in \mathcal{S}_M^{(k)}$ with $|\Gamma(\boldsymbol{j}) \cap S| = 1$. We can write $h_S = h_{\boldsymbol{j}'} h_{S \setminus \{\boldsymbol{j}'\}}$ where $\boldsymbol{j}' \in \Gamma(\boldsymbol{j}) \cap S$. The summation includes another pair with $\boldsymbol{j}' \in V_M$ and $S' = \{\boldsymbol{j}\} \cup (S \setminus \{\boldsymbol{j}'\}) \in \mathcal{S}_M^{(k)}$. These pairs cancel:

$$h_{\boldsymbol{j}} h_S + h_{\boldsymbol{j}'} h_{S'} = (h_{\boldsymbol{j}} h_{\boldsymbol{j}'} + h_{\boldsymbol{j}'} h_{\boldsymbol{j}}) h_{S \setminus \{\boldsymbol{j}'\}} = 0. \tag{34}$$

Cancellation of the second term: This is a new feature of our model. Consider $\boldsymbol{j} = \boldsymbol{c} \in V_M$ and $S \in \mathcal{S}_M^{(k)}$ with $|\Gamma(\boldsymbol{c}) \cap S| = 3$, meaning $h_{\boldsymbol{c}}$ is a claw center with leaves $\mathcal{L}_{\boldsymbol{c}}^t \subset S$ for some $t \in \{A, B\}$. Since the leaves form an independent set, they can be simultaneously included in S.

We can decompose $h_S = h_{h_{\boldsymbol{c}}^{\mathcal{L},t,1}} h_{h_{\boldsymbol{c}}^{\mathcal{L},t,2}} h_{h_{\boldsymbol{c}}^{\mathcal{L},3}} h_{S \setminus \mathcal{L}_{\boldsymbol{c}}^t}$. Define $\boldsymbol{c}' = \overline{2m+3}$ if $\boldsymbol{c} = 2m-1$, and vice versa. For $\boldsymbol{d} \in \{\boldsymbol{c}, \boldsymbol{c}'\}$ and $\tau \in \{A, B\}$, define $S_{\boldsymbol{d},\tau} \equiv \mathcal{L}_{\boldsymbol{d}}^{\tau} \cup (S \setminus \mathcal{L}_{\boldsymbol{c}}^t)$.

The summation includes all four pairs $(\boldsymbol{d}, S_{\boldsymbol{d},\tau})$ (see Appendix A.2.6 for details). These cancel as follows:

$$\begin{aligned} \sum_{\boldsymbol{d} \in \{\boldsymbol{c}, \boldsymbol{c}'\}} \sum_{\tau \in \{A,B\}} h_{\boldsymbol{d}} h_{S_{\boldsymbol{d},\tau}} &= \sum_{\tau \in \{A,B\}} \left[h_{\boldsymbol{c}} h_{h_{\boldsymbol{c}}^{\mathcal{L},\tau,1}} h_{h_{\boldsymbol{c}}^{\mathcal{L},\tau,2}} h_{h_{\boldsymbol{c}}^{\mathcal{L},3}} + h_{\boldsymbol{c}'} h_{h_{\boldsymbol{c}'}^{\mathcal{L},\tau,1}} h_{h_{\boldsymbol{c}'}^{\mathcal{L},\tau,2}} h_{h_{\boldsymbol{c}'}^{\mathcal{L},3}} \right] h_{S \setminus \mathcal{L}_{\boldsymbol{c}}^t} \\ &= (\mathbb{A}_{2m-1} \mathbb{C}_{2m+2} - \mathbb{C}_{2m} \mathbb{A}_{2m+3}) h_{S \setminus \mathcal{L}_{\boldsymbol{c}}^t} \\ &= 0, \end{aligned} \tag{35}$$

where the last equality follows from the relation (19). □

The next theorem establishes that the higher-order charges are mutually commuting:

Theorem 2. *The charges* (29) *mutually commute:*

$$[Q_M^{(k)}, Q_M^{(l)}] = 0 \quad \forall k, l \in \{1, 2, \ldots, S_M\}. \tag{36}$$

The proof of Theorem 2 is given in Appendix A. While it requires a more careful analysis of the frustration graph, the essential point remains the same: the relation (19) plays a crucial role.

4.3 Recursion for the higher-order charges

We here show the recursion relations that the higher-order charges satisfy. We can define similar quantities to those in (29) when given a frustration graph G that is a subgraph of $G_M = (V_M, E_M)$ for some M. Let $\mathcal{S}_G^{(k)}$ denote the collection of all independent sets of order k in

G. We also define a *pseudo-charge* that reproduces the charges (29) for the appropriate choice of frustration graph G:

$$Q_G^{(k)} \equiv \sum_{S \in \mathcal{S}_G^{(k)}} h_S, \tag{37}$$

where we have used the abbreviated notation (31). Note that $\{Q_G^{(k)}\}_{k=1,2,\dots}$ are not necessarily mutually commuting charges. They form a set of mutually commuting charges when the frustration graph is a free fermionic (Figure 8 and 18).

The pseudo-charge (37) satisfies the following recursion:

$$Q_G^{(k)} = Q_{G\setminus K}^{(k)} + \sum_{\boldsymbol{j} \in K} h_{\boldsymbol{j}} Q_{G\setminus\Gamma[\boldsymbol{j}]}^{(k-1)}, \tag{38}$$

where K is a clique in G. The proof of (38) follows trivially from the definition of the pseudo-charge (37). Please refer to [7,8] for a more detailed explanation.

Using the recursion for the pseudo-charges (38), we can derive the following recursion for the charges (29):

$$\begin{aligned} Q_{2m}^{(k)} = Q_{2m-1}^{(k)} &+ h_{2m} Q_{2m-3}^{(k-1)} + h_{\overline{2m+1}} Q_{2m-4}^{(k-1)} \\ &+ h_{2m-2} h_{\overline{2m+1}} Q_{2m-6}^{(k-2)} + h_{2m-5} h_{\overline{2m+1}} Q_{2m-8}^{(k-2)}, \end{aligned} \tag{39}$$

and

$$Q_{2m-1}^{(k)} = Q_{2m-2}^{(k)} + h_{2m-1} Q_{2m-4}^{(k-1)}. \tag{40}$$

The initial conditions are $Q_0^{(0)} = Q_{-1}^{(0)} = Q_{-2}^{(0)} = \mathbb{1}$ and $Q_m^{(k)} = 0$ for $k < 0$ and $Q_m^{(k)} = 0$ for $m < 0$ and $k > 0$. The proofs of (39) and (40) are given in Appendix B. From these charge recursions, we can confirm that $S_M = \lfloor (M+2)/3 \rfloor$.

5 Transfer matrix

In this section, we introduce the transfer matrix for the Hamiltonian (24), from which we can derive the polynomial for the excitation spectrum. We define the transfer matrix from the conserved charges (29) as

$$T_M(u) \equiv \sum_{k \geq 0} (-u)^k Q_M^{(k)}, \tag{41}$$

where u is the spectral parameter.

The transfer matrix satisfies the following recursion relations for even and odd M, respectively:

$$\begin{aligned} T_{2m}(u) = &T_{2m-1}(u) - u h_{2m} T_{2m-3}(u) - u h_{\overline{2m+1}} T_{2m-4}(u) \\ &+ u^2 h_{2m-2} h_{\overline{2m+1}} T_{2m-6}(u) + u^2 h_{2m-5} h_{\overline{2m+1}} T_{2m-8}(u), \end{aligned} \tag{42}$$

and

$$T_{2m-1}(u) = T_{2m-2}(u) - u h_{2m-1} T_{2m-4}(u). \tag{43}$$

The initial conditions are $T_0(u) = T_{-2}(u) = \mathbb{1}$, with the convention that $h_m = h_{\overline{2m-1}} = 0$ for all $m \leq 0$. The recursion relations for the transfer matrix (42) and (43) follow directly from the recursions for the charges (39) and (40).

In the limit of the FFD model we set $h_{\bar{k}} \equiv 0$, and we get the recursion relation of the FFD model [4] :

$$T_k(u) = T_{k-1}(u) - u h_k T_{k-3}(u). \tag{44}$$

Substituting the two above equations above into each other we obtain the recursion relation only contains the even M transfer matrix:

$$T_{2m}(u) = T_{2m-2}(u) - u \mathbb{S}_{2m} T_{2m-4}(u) + u^2 \mathbb{A}_{2m-1} T_{2m-6}(u) + u^2 \mathbb{C}_{2m-2} T_{2m-8}(u)\,, \tag{45}$$

where we defined

$$\mathbb{S}_{2m} \equiv h_{2m-1} + h_{2m} + h_{\overline{2m+1}}\,. \tag{46}$$

One can further simplify this recursion substantially to read

$$T_{2m}(u) = T_{2m-2}(u) - \frac{u}{2}\{\mathbb{S}_{2m}, T_{2m-2}(u)\}, \tag{47}$$

as shown in Appendix E.1.

The following theorem provides the polynomial whose roots determine the free fermionic spectrum:

Theorem 3. *The transfer matrix satisfies the following simple inversion relation*

$$T_M(u) T_M(-u) = P_M(u^2) \cdot \mathbb{1} \tag{48}$$

where $P_M(z)$ is a polynomial of degree S_M. For even M it satisfies the following recursion:

$$P_{2m}(u^2) = P_{2m-2}(u^2) - u^2 \mathbb{S}_{2m}^2 P_{2m-4}(u^2) + u^4 \mathbb{A}_{2m-1}^2 P_{2m-6}(u^2) - u^4 \mathbb{C}_{2m-2}^2 P_{2m-8}(u^2)\,. \tag{49}$$

For the case of $P_M(u^2)$ with odd M, we have

$$P_{2m-1}(u^2) = P_{2m-2}(u^2) - u^2 b_{2m-1}^2 P_{2m-4}(u^2)\,. \tag{50}$$

The starting point is $P_0(u^2) = P_{-2}(u^2) = 1$ such that $b_m = b_{\overline{2m-1}} = 0$, $\forall m \leq 0$ formally.

In Appendix C, we provide the proof of Theorem 3. We note that the following quantities appearing in (49) in Theorem 3 are all scalars:

$$\mathbb{S}_{2m}^2 = b_{2m-1}^2 + b_{2m}^2 + b_{\overline{2m+1}}^2\,, \tag{51}$$

$$\mathbb{A}_{2m-1}^2 = (b_{2m-3} b_{2m} \pm b_{2m-2} b_{\overline{2m+1}})^2\,, \tag{52}$$

$$\mathbb{C}_{2m-2}^2 = b_{2m-3}^2 b_{\overline{2m+3}}^2\,, \tag{53}$$

where the sign factor in the second line is determined by which sign we choose for the central element μ_{2m-1} in (14).

In appendix D, we give the proof for $S_M = \lfloor (M+2)/2 \rfloor$ using the recursion for the polynomial (49) and (50).

6 Free fermions

In this section, we derive the free fermionic operators for the Hamiltonian (7). First we introduce the simplicial mode and corresponding simplicial clique. Then, we construct the free fermion modes using the simplicial mode and simplicial clique.

The simplicial mode and clique are localized around one of the boundaries of the spin chain. Correspondingly, there are two ways to proceed, by choosing either boundary. The Hamiltonian is not space reflection symmetric, therefore the two cases will be genuinely different. This is in contrast with the situation in the original FFD model, where the two boundaries of the chain were equivalent.

Although in the following we only treat the Hamiltonian (7), whose frustration graph is given in Figure 7 and which is a special case of the more general Hamiltonian (24), the free fermion solution can be constructed in the same way for the general case.

6.1 Simplicial cliques and simplicial modes

We now introduce two key structures that are central to our free-fermion solution, referring to the explanation in [4,8]. A *simplicial clique* K_s is a clique with the additional property that, for every vertex $v \in K_s$, the neighborhood of v outside K_s induces a clique in $G \setminus K_s$. More precisely, for each $v \in K_s$, the set $\Gamma(v) \setminus K_s$ forms a clique. A graph is called *simplicial* if it contains at least one simplicial clique. For a simplicial clique K_s in G, we can define for each $v \in K_s$ the clique $K_v = (\Gamma(v) \setminus K_s) \cup \{v\}$, such that $\Gamma[v] = K_s \cup K_v$. All frustration graphs treated in this paper are simplicial.

Associated with each simplicial clique, we define a *simplicial mode*. A simplicial mode with respect to K_s is a additional generator χ which anticommutes only with the generators corresponding to vertices in K_s. The simplicial mode acts as a seed for constructing the fermionic eigenmodes. By repeatedly commuting χ with the Hamiltonian, we generate a Krylov subspace whose structure is intimately connected to the induced path tree rooted at the simplicial clique. This connection between the algebraic structure (commutation relations) and the graph structure (induced paths) is what enables the exact free-fermion solution.

In the following, we show the simplicial mode for our frustration graph (Figure 7).

6.2 Right-end simplicial mode

First, we define the simplicial mode at the right-end of the chain. In this case, the definition of simplicial mode differs for even M and odd M. The simplicial mode for even M is

$$\{\chi_M, h_M\} = \{\chi_M, h_{M-1}\} = 0\,, \quad [\chi_M, h_l] = 0 \quad (l < M-1)\,. \tag{54}$$

The simplicial mode for odd M is the same as the original FFD case [4] :

$$\{\chi_M, h_M\} = 0\,, \quad [\chi_M, h_l] = 0 \quad (l < M)\,. \tag{55}$$

Then, the corresponding simplicial clique is

$$K_M^{(s)} \equiv \begin{cases} \{M-1, M, \overline{M+1}\} & M \text{ is even} \\ \{M\} & M \text{ is odd} \end{cases}\,. \tag{56}$$

6.3 Left-end simplicial mode

Next, we explain the simplicial mode at the left end of the chain. In this case, the definition of the simplicial mode is the same for both even and odd M. The simplicial mode is defined by

$$\{\chi_M, h_1\} = \{\chi_M, h_2\} = 0\,, \quad [\chi_M, h_l] = 0 \quad (2 < l)\,. \tag{57}$$

Then, the corresponding simplicial clique is

$$K_M^{(s)} \equiv \{1, 2\}\,. \tag{58}$$

6.4 Construction of the free fermion mode

Here we construct the free fermion mode using the simplicial clique introduced above. We can use either of the left-end and right-end simplicial mode.

We would like to prove that the operators

$$\Psi_k \equiv \frac{T_M(-u_k)\chi_M T_M(u_k)}{\mathcal{N}_k} \tag{59}$$

act as fermionic ladder operators that satisfy the eigenvalue problem of the adjoint action with the Hamiltonian as

$$[H, \Psi_k] = 2\epsilon_k \Psi_k, \tag{60}$$

where $\epsilon_k = u_k^{-1}$ are the energies of the fermion modes, and the u_k-s are the roots of the polynomials $P_M(u_k^2) = 0$ in (48). As the latter come in opposite-sign pairs, we may define $u_{-k} = -u_k$ where $u_k > 0$ for $k = 1, 2, \ldots, S_M$. The $\Psi_k^\dagger = \Psi_{-k}$ are creating while Ψ_k are annihilating a fermionic mode with positive energy for $k \geq 1$. They also need to anticommute as

$$\{\Psi_k, \Psi_{-k'}\} = \delta_{k,k'} \cdot \mathbb{1} \tag{61}$$

where the $k = k'$ case sets the normalization constant $\mathcal{N}_k$ in (59). Below we will show how the basic properties of the simplicial mode (edge operator) and the recursion for the transfer matrix lead to the above statements.

We start from the trivial identity

$$[H_M, T_M(-u)\chi_M T_M(u)] = 2 \sum_{v \in K_M^{(s)}} T_M(-u) h_v \chi_M T_M(u)\,, \tag{62}$$

that follows from commuting H_M through the transfer matrices due to Theorem 1, and the properties of the simplicial mode. Then we apply the next theorem to arrive at (60).

Lemma 1. *The following modified inversion relation holds:*

$$T_M(-u)\left(1 - u \sum_{v \in K_M^{(s)}} h_v\right)\chi_M T_M(u) = P_M(u^2)\left(1 + u \sum_{v \in K_M^{(s)}} h_v\right)\chi_M\,. \tag{63}$$

The proof of Lemma 1 is given in Appendix E.1. Then, we have the following theorem:

Theorem 4. *The fermionic operators defined by (59) satisfy the anticommutation relations and also the commutation relation (60).*

Proof. Replacing the term on the l.h.s. of (63) that appears on the r.h.s. of (62) using the latter relation gives

$$[H_M, T_M(-u)\chi_M T_M(u)] = 2u^{-1}T_M(-u)\chi_M T_M(u) - 2P_M(u^2)\left(u^{-1} + \sum_{v\in K_M^{(s)}} h_v\right)\chi_M, \quad (64)$$

and evaluating it at a root u_k of the polynomial $P_M(u_k^2) = 0$ we get (60) (up to the undetermined normalization factor $\mathcal{N}_k$). For the proof of the canonical anticommutations in (61) see Appendix E.2. □

As the number of fermionic modes obtained this way depends on the number of roots of the polynomial $P_M(u^2)$, their number is S_M. The number of the different energy levels is thus $2^{\lfloor (M+2)/3 \rfloor}$ and since the dimension of the Hilbert space is 2^M it means the energy eigenstates are exponentially degenerate. An understanding of these degeneracies in the case of the FFD model has been achieved in [15].

Following the arguments of Section 3.4 in [4] moreover using (48) and (145) it is possible to show that the basis of fermionic modes is complete in the sense, that one can reconstruct the Hamiltonian and the transfer matrix itself as

$$H = \sum_{k=1}^{S_M} \epsilon_k[\Psi_k, \Psi_{-k}], \qquad T_M(u) = \prod_{k=1}^{S_M} (1 - u\epsilon_k[\Psi_k, \Psi_{-k}]) \,. \quad (65)$$

Note that similarly to [14] we may extend our fermion algebra by a Majorana zero mode Ψ_0, that only exists for certain system sizes. If it exists, it may be defined as the $u \to \infty$ limit

$$\Psi_0 \equiv \frac{1}{2C_0}\left(\chi_M + \lim_{u\to\infty} \frac{T_M(-u)\chi_M T_M(u)}{P_M(u^2)}\right), \quad (66)$$

where C_0 is a known constant defined in (69). It satisfies the following properties:

$$[H, \Psi_0] = 0, \quad \Psi_0^2 = \mathbb{1}, \quad \text{and} \quad \{\Psi_0, \Psi_k\} = 0 \text{ for } k = \pm 1, \pm 2, \ldots, \pm S_M. \quad (67)$$

Although the zero mode is not needed for the reconstruction of the Hamiltonian and the transfer matrix in (65) (due to its zero energy $\epsilon_0 = 0$), as we will see in Section 7, it appears in the decomposition of the simplicial mode.

7 Correlation functions

So far we obtained the solution of the Hamiltonian in terms of the fermionic operators. As a next step we can also compute certain correlation functions, namely the correlations of those operators which take a sufficiently simple form in terms of the fermions. This was achieved in [14] for the FFD model, and now we generalize that formalism to our model.

The first step is solving the inverse problem for the edge operator in Subsection 6.2, i.e. decomposing it into the fermion modes:

$$\chi_M = \sum_{k=-S_M}^{S_M} C_k \Psi_k, \quad (68)$$

where the coefficients C_k read

$$C_j = \sqrt{\frac{P_{M-r_M}(u_j^2)}{-u_j^2 P'_M(u_j^2)}} \quad \text{for } j \neq 0\,, \tag{69}$$

and

$$C_0 = \sqrt{\lim_{M\to\infty} \frac{P_{M-r_M}(u^2)}{P_M(u^2)}}\,, \tag{70}$$

with $r_{2m} = 2$ and $r_{2m+1} = 1$. The zero mode is not present if $S_{M-r_M} < S_M$, in this case $C_0 = 0$. We may calculate infinite temperature correlators $\langle\cdot\rangle \equiv \mathrm{Tr}(\cdot)/\mathrm{Tr}(\mathbb{1})$ of certain operators defined by the recursion

$$o_j = \frac{1}{2}[H, o_{j-1}], \quad o_0 \equiv \chi_M \tag{71}$$

that are elements of the Krylov-subspace generated by repeated action of the commutator with the Hamiltonian. Using (68), their time evolution reads

$$o_j(t) = e^{iHt} o_j e^{-iHt} = \sum_{k=-S_M}^{S_M} C_k \epsilon_k^j e^{2i\epsilon_k t} \Psi_k, \tag{72}$$

and it is useful to define their anticommutator that is proportional to the identity

$$\{o_{j_1}(t_1), o_{j_2}(t_2)\} \equiv 2B_{j_1,j_2}(t_1 - t_2)\mathbb{1}. \tag{73}$$

It is easy to show that Wick theorem leads to

$$\begin{aligned}\langle o_{j_1}(t_1) o_{j_2}(t_2) o_{j_3}(t_3) o_{j_4}(t_4)\rangle = B_{j_1,j_2}(t_{1,2}) B_{j_3,j_4}(t_{3,4}) - B_{j_1,j_3}(t_{1,3}) B_{j_2,j_4}(t_{2,4}) \\ + B_{j_1,j_4}(t_{1,4}) B_{j_2,j_3}(t_{2,3})\end{aligned} \tag{74}$$

where $t_{i,j} \equiv t_i - t_j$, and the function

$$B_{j_1,j_2}(t) = \frac{(-1)^{j_2}}{(2i)^{j_1+j_2}} \partial_t^{j_1+j_2} B(t) \tag{75}$$

can be easily calculated from the self-correlator of the edge operator that reads as as

$$B(t) \equiv B_{0,0}(t) = \langle \chi_M(t) \chi_M(0)\rangle = \sum_{j=0}^{S_M} C_j^2 \cos(2\epsilon_j t). \tag{76}$$

One of the simplest operators one may construct from bilinears of the Krylov subspace looks like

$$\mathbb{S}_M \equiv o_1 o_0 = \begin{cases} h_{2m-1} & M = 2m-1 \\ h_{2m-1} + h_{2m} + h_{\overline{2m+1}} & M = 2m \end{cases} \tag{77}$$

that directly corresponds to the simplicial clique in (56) of the frustration graph. The self-correlator of this operator is then

$$\langle \mathbb{S}_M(t) \mathbb{S}_M(0)\rangle = \frac{1}{4}\left(\dot{B}^2(t) - \ddot{B}(t) B(t)\right) \tag{78}$$

where the dot means time-derivative and the correlator may be calculated very efficiently using (76) and (69) after solving for the roots of the polynomial $P_M(u^2)$.

In case of Floquet time evolution with the unitary circuit $\mathcal{V}(\delta) \equiv T_M(-i\delta)/\sqrt{P_M(-\delta^2)}$ the fermion modes pick up the phase

$$\mathcal{V}^\dagger(\delta)\Psi_j\mathcal{V}(\delta) = \frac{T_M(-i\delta)\Psi_j T_M(i\delta)}{P_M(-\delta^2)} = \frac{u_j + i\delta}{u_j - i\delta}\Psi_j = e^{2i\arctan(\epsilon_j\delta)}\Psi_j \tag{79}$$

after each application of the circuit. After the N^{th} time step (that is, total time $t = N\delta$ in the Trotterization picture of [14]), the phase angle acquired is $\theta_j = 2N\arctan(\epsilon_j\delta)$. This is in comparison to real time evolution, where the same angle is simply $\theta_j = 2\epsilon_j t$. Analogously to (72) the Krylov-basis elements can be time-evolved as $o_j(t = N\delta) = \left(\mathcal{V}_M^\dagger(\delta)\right)^N o_j \mathcal{V}_M^N(\delta)$ and formula (74) describes their correlators by a formal substitution of the phase angles $2\epsilon_k t \to 2N\arctan(\epsilon_k\delta)$. That means the building blocks for the correlators for both real and Floquet time evolution are

$$B_{j_1,j_2}(t) = \sum_{k=1}^{S_M} C_k^2 \epsilon_k^{j_1+j_2} \frac{(-1)^{j_2}e^{i\theta_k} + (-1)^{j_1}e^{-i\theta_k}}{2}, \quad \forall\ j_1 + j_2 > 0, \tag{80}$$

while $B(t) = \sum_{k=0}^{S_M} C_k^2 \cos(\theta_k)$, with the respective phase angles θ_k as explained above.

8 Factorization of the transfer matrix

In this Section we show that a special case of the transfer matrix (41) becomes proportional to a quantum unitary circuit with free fermions in disguise reported in [13]. In fact, finding the Hamiltonian behind the quantum circuit of [13] was one of the motivations for the present work.

First we consider the factorization of our transfer matrix into the product of local operators as

$$\mathcal{V}_M = G_M \cdot G_M^\top , \tag{81}$$

where

$$\begin{aligned} G_{2k} =& (g_2 g_4 \cdots g_{2k})(g_1 g_3 g_5 \cdots g_{2k-1}) && (82)\\ =& (g_2 g_1)(g_4 g_3)\cdots(g_{2k}g_{2k-1})\,, && (83) \end{aligned}$$

and the local gates g_j are defined as

$$g_j \equiv \cos(\theta_j/2) + \sin(\theta_j/2) b_j^{-1} h_j\,, \tag{84}$$

where for odd M, we define $G_{2k-1} \equiv G_{2k}\big|_{\theta_{2k}=0}$. The subscript $\top$ denotes the transpose operation, with $g_j^\top = g_j$. Hereafter, for notational clarity, the explicit dependence on θ_j will be suppressed unless otherwise specified.

Our notation differs slightly from the original paper [13]. The notation used in Ref. [13] can be recovered by $\mathcal{V}_{2k}\big|_{\theta_1=\theta_{2k}=0}$ and subsequently applying the index shift $j \to j-1$.

The formula (81) is analogous to the factorization of the transfer matrix in the original FFD model [4] . The only difference is the ordering of the local operators in (83). The work [13] asked the question: which operator orderings are compatible with the free fermionic structures, and the special ordering of (83) was found to be the simplest possibility different from the original one in [4] .

The local gates in (84) are not unitary. However, we can have unitary gates using the transformation of (5.10) in [13], which amounts to an analytic continuation in the angles. Using this transformation we provide a rigorous proof of the conjecture in [13] that one of the quantum circuit proposed in [13] is indeed free fermionic.

Theorem 5. *If the parameters b_j are chosen arbitrarily, the parameters β_1 and β_3 are set by*

$$\beta_1 = \frac{1}{1-b_2^2}\,, \qquad \beta_3 = \frac{1}{1-b_2^2-b_4^2}\,. \tag{85}$$

and the remaining β_{2j-1} are calculated using (8), then the transfer matrix can be factorized at the special point $u=-1$. More precisely we obtain

$$T_{2k}(u=-1) = \mathcal{V}_{2k}\,, \tag{86}$$

where the angles are determined by the recursion relation:

$$\begin{aligned} \sin\theta_{2j} &= \frac{b_{2j}}{\cos\theta_{2j-2}}\,, \\ \sin\theta_{2j-1} &= \frac{b_{2j-1}}{\cos\theta_{2j-2}\cos\theta_{2j-3}\cos\theta_{2j}}\,, \end{aligned} \tag{87}$$

where $\theta_0 = \theta_{-1} = \theta_{M+1} = 0$. For the relation between the parameters β_{2j-1} and the angles we obtain the direct relation

$$\beta_{2j-1} = \frac{1}{\cos^2\theta_{2j-2}\cos^2\theta_{2j}}\,. \tag{88}$$

which is compatible with (8).

Proof. We derive the recursion equation for the quantum circuit (81) and see that recursion is the same as that we derived above (43)-(42). We can prove the transfer matrix satisfies the following recursion relation:

$$\begin{aligned} \mathcal{V}_{2k} &= \mathcal{V}_{2k-2} + (c_{2k-2}h'_{2k} + c_{2k}c_{2k-2}c_{2k-3}h'_{2k-1} + c_{2k-5}h'_{2k-2}h'_{2k-3}h'_{2k})\mathcal{V}_{2k-4} \\ &\quad + c_{2k-4}c_{2k-5}h'_{2k}h'_{2k-3}\mathcal{V}_{2k-6} + c_{2k-4}c_{2k-5}c_{2k-6}c_{2k-7}h'_{2k-5}h'_{2k-2}h'_{2k-3}h'_{2k}\mathcal{V}_{2k-8}\,, \end{aligned} \tag{89}$$

$$\mathcal{V}_{2k-1} = \mathcal{V}_{2k-2} + c_{2k-2}c_{2k-3}h'_{2k-1}\mathcal{V}_{2k-4}\,. \tag{90}$$

where we denote $c_j \equiv \cos\theta_j$ and $h'_j \equiv \sin\theta_j b_j^{-1} h_j$. The equation in the second line (90) is identical to that of the original FFD paper [4] and can be derived in the same manner. The proof of the first line (89) is provided in the Appendix F. By eliminating the angles θ_j from the above equation using (87) and (88), we can identify the above recursion (89) with the recursion relation for the transfer matrix (42) with $u=-1$.

Since the recursion equation is identical and the initial condition is the same, we can conclude that the two transfer matrices coincide due to the uniqueness of the solution to the recursion equation, thus proving (86). □

We also attempted to find a factorization of the transfer matrix for generic values of the spectral parameter, however we have not yet found a general solution. This is left for further work.

9 Conclusion

We introduced a new spin chain model that can be solved with free fermions in disguise, despite its frustration graph containing both claws and even holes—structures that violate the sufficient conditions established in previous works [7,8]. The free fermionic solvability is achieved through carefully constructed algebraic relations among the coupling constants, which we derived by introducing an extension of the FFD algebra.

Our Hamiltonian can be formulated solely within the original FFD algebra for a special case, distinguishing it from other extensions such as [12]. When specific coupling constants are set to zero, our model reduces to the original FFD model. Moreover, for a particular choice of parameters, the transfer matrix can be factorized into a product of three-site operators, yielding a quantum circuit first introduced in [13]. That circuit was conjectured to be free fermionic, and our construction now proves that conjecture.

We also attempted to factorize the transfer matrix for the general case but did not succeed. This remains an open problem.

In future work, it would be interesting to prove the free fermionic nature of other circuits presented in [13], and eventually to develop a more general theory for such circuits.

An even more challenging task is to derive sufficient conditions for free fermionic solvability when the standard conditions of [7,8] are not applicable. The present model and [12] are examples where special algebraic relations guarantee integrability. It would be desirable to uncover similar examples or to develop a general theory for this problem.

To our knowledge, this is the first example of free fermions in disguise with both claws and even holes simultaneously.

Acknowledgements

The authors thank H. Katsura for helpful discussions. K.F. was supported by MEXT KAKENHI Grant-in-Aid for Transformative Research Areas A "Extreme Universe" (KAKENHI Grant No. JP21H05191). This research was supported by the Hungarian National Research, Development and Innovation Office: I.V. and B.P. were supported by the NKFIH Grant No. K-145904, also B.P. was supported by the NKFIH excellence grant TKP2021-NKTA-64.

A Proof of mutual commutativity of charges

In this appendix, we prove the mutual commutativity of the charges in Eq. (29). In the following, we often omit the subscript of the number of the generators M. Following Eq. (31), for any independent set $S \subset V_M$, we define $h_S \equiv \prod_{\boldsymbol{j} \in S} h_{\boldsymbol{j}}$.

For any independent sets $S, S' \subset V_M$, we have

$$[h_S, h_{S'}] = \begin{cases} 2h_S h_{S'} & \text{if } |E_{S\oplus S'}| \text{ is odd} \\ \\ 0 & \text{if } |E_{S\oplus S'}| \text{ is even} \end{cases}, \tag{91}$$

where $S \oplus S' \equiv (S \cup S') \setminus (S \cap S')$ denotes the symmetric difference. Note that the product can be rewritten as $h_S h_{S'} = \left(\prod_{\boldsymbol{j} \in S\cap S'} b_{\boldsymbol{j}}^2\right) h_{S\setminus S'} h_{S'\setminus S}$ where the operators on common vertices become scalar factors.

The commutator of the charges then reads

$$\left[Q_M^{(k)}, Q_M^{(l)}\right] = \left[\sum_{L\in\mathcal{S}_M^{(k)}} h_L, \sum_{R\in\mathcal{S}_M^{(l)}} h_R\right] = 2 \sum_{\substack{(L,R)\in\mathcal{S}_M^{(k)}\times\mathcal{S}_M^{(l)} \\ |E_{L\oplus R}| \text{ is odd}}} h_L h_R \,. \tag{92}$$

We show that all terms in the RHS cancel. For this, we consider the following subsets of $E_{L\oplus R}$: (i) *balanced-odd-edges components* (BOE components) and (ii) *claw-cancellation parts* (CC parts). We prove that the cancellation is ensured if $E_{L\oplus R}$ includes either at least one BOE component or at least one CC part. Since $|E_{L\oplus R}|$ is odd, at least one of these structures must exist.

Below, we explain the two cases of cancellation. All terms in the RHS of (92) cancel via either BOE components or CC parts. In Appendix A.1, we define BOE component and we show that when $L\oplus R$ has the BOE component, there exists the other term that cancels $h_L h_R$. In Appendix A.2, we define CC-part and show that when $L\oplus R$ has the CC-part, there exists the other three terms that cancel with $h_L h_R$. In Appendix A.3, we show all terms are canceled at least by either BOE components or CC parts.

A.1 Cancellation via balanced-odd-edges components

We define a subset $\mathcal{O}\subset L\oplus R$ to be a BOE component if it satisfies the following conditions: (i) $|E_{\mathcal{O}}|$ is odd, (ii) $|\mathcal{O}\cap L| = |\mathcal{O}\cap R|$, and (iii) $G[\mathcal{O}]$ is an isolated connected subgraph in $G[L\oplus R]$.

When $L\oplus R$ contains a BOE component $\mathcal{O}$, there exists another pair $(L',R')\in\mathcal{S}_M^{(k)}\times\mathcal{S}_M^{(l)}$ defined by

$$L'\equiv(L\setminus\mathcal{O}_L)\cup\mathcal{O}_R,\quad R'\equiv(R\setminus\mathcal{O}_R)\cup\mathcal{O}_L, \tag{93}$$

where $\mathcal{O}_L\equiv\mathcal{O}\cap L$ and $\mathcal{O}_R\equiv\mathcal{O}\cap R$. Note that the following anticommutation relation holds:

$$h_{\mathcal{O}_L}h_{\mathcal{O}_R}+h_{\mathcal{O}_R}h_{\mathcal{O}_L}=0, \tag{94}$$

because there are an odd number of edges between $\mathcal{O}_L$ and $\mathcal{O}_R$, and both $\mathcal{O}_L$ and $\mathcal{O}_R$ are independent sets. Then we have the following cancellation:

$$h_L h_R + h_{L'}h_{R'} = h_{L\setminus\mathcal{O}_L}(h_{\mathcal{O}_L}h_{\mathcal{O}_R}+h_{\mathcal{O}_R}h_{\mathcal{O}_L})h_{R\setminus\mathcal{O}_R}=0. \tag{95}$$

Thus, we have proved that the term $h_L h_R$ in the RHS of (92) cancels with the term $h_{L'}h_{R'}$ if $L\oplus R$ contains a BOE component.

Note that the cancellation via BOE components follows the same argument as in the claw-free case [7]. Next, we consider the cancellation arising from CC parts in $L\oplus R$.

A.2 Cancellation via claw-cancellation part

Here we explain the cancellation of the term $h_L h_R$ in the RHS of (92) for the case when $L\oplus R$ has a claw-cancellation part (CC-part). We first explain the structure of the claw. Then, we define the claw-cancellation part. And finally, we show the cancellation arising from the claw-cancellation part.

A.2.1 Structure of claw

First, we explain the claw structure. Please refer to Section 3.2 for the definitions of the notation for claws. Since the leaves form an independent set, they can be simultaneously included in L (or R).

We show the structure of claws at h_{2j-1} ($h_{\overline{2j+3}}$) in Figure 9 (Figure 10). To facilitate understanding of the neighbors of claws at center h_{2j-1} ($h_{\overline{2j+3}}$), we illustrate the neighborhood structure in Figure 11 (Figure 12), which is closely explained in the next section A.2.2. In these figures, bold green lines indicate edges connecting the claw center to its leaves. The claw centers are represented by grayish-blue-filled circles, while the leaves are shown as green-filled circles. We assume the claw center belongs to $L\in S^{(k)}$ and the leaves belong to $R\in S^{(l)}$; the converse case follows by a similar argument.

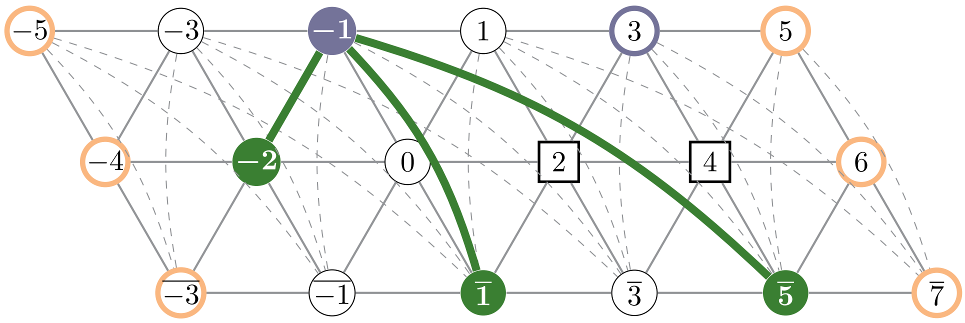

type A claw at h_{2j-1}

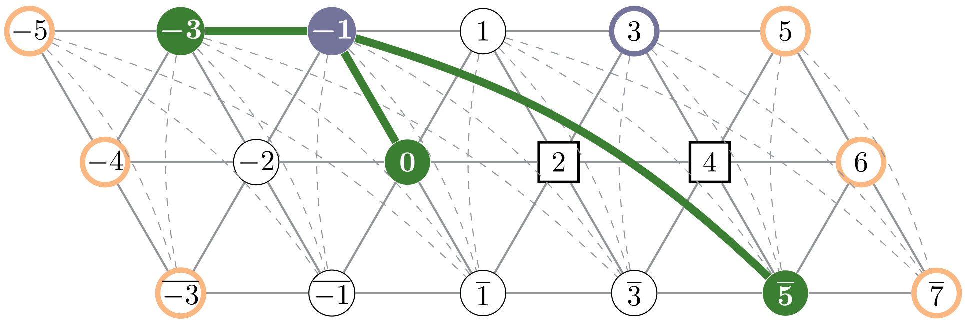

type B claw at h_{2j-1}

Figure 9: Structures of claws at h_{2j-1}. The bold green edges connect the claw center to the claw leaves, while gray edges indicate all other edges on the frustration graph. Each vertex labeled with number i represents h_{2j+i} and labeled with $\bar{i}$ represents $h_{\overline{2j+i}}$. The grayish-blue-filled circle indicates the claw center h_{2j-1}. Green-filled circles indicate the claw leaves: h_{2j-2}, $h_{\overline{2j+1}}$, $h_{\overline{2j+5}}$ for type A claws, and h_{2j-3}, h_{2j}, $h_{\overline{2j+5}}$ for type B claws. Rectangles represent the frozen even vertices h_{2j+2} and h_{2j+4}. The grayish-blue-bordered circle indicates the special odd vertex h_{2j+3}. Orange-bordered circles indicate the rearrangeable clique: $\mathcal{R}^-_{2j-1} = \{h_{2j-5}, h_{2j-4}, h_{\overline{2j-3}}\}$ on the left, and $\mathcal{R}^+_{2j-1} = \{h_{2j+5}, h_{2j+6}, h_{\overline{2j+7}}\}$ on the right, which is the same as those in Figure 9. The white circles indicate forbidden vertices, that cannot be connected to any of the claw leaves in $L \oplus R$.

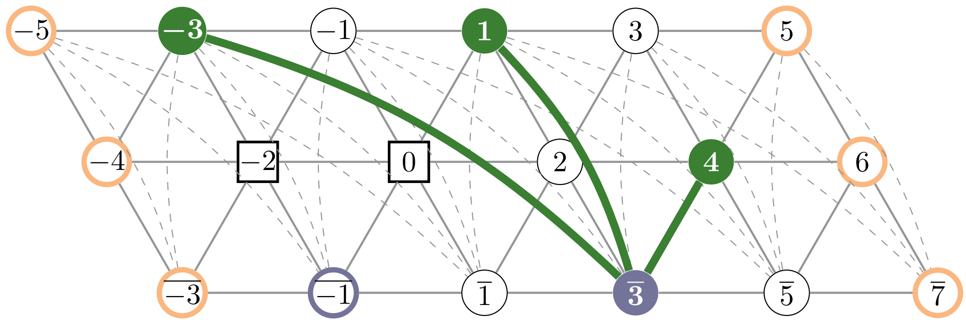

type A claw at $h_{\overline{2j+3}}$

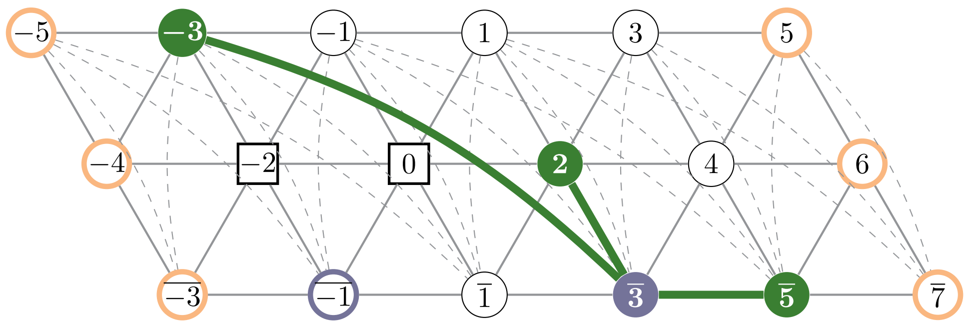

type B claw at $h_{\overline{2j+3}}$

Figure 10: Structures of claws at $h_{\overline{2j+3}}$. The bold green edges connect the claw center to the claw leaves, while gray edges indicate all other edges. Each vertex labeled with number i represents h_{2j+i} and labeled with $\bar{i}$ represents $h_{\overline{2j+i}}$. The grayish-blue-filled circle indicates the claw center $h_{\overline{2j+3}}$. Green-filled circles indicate the claw leaves: h_{2j-3}, h_{2j+1}, h_{2j+4} for type A claws, and h_{2j-3}, h_{2j+2}, $h_{\overline{2j+5}}$ for type B claws. Solid rectangles represent the frozen even vertices h_{2j-2} and h_{2j}. The grayish-blue-bordered circle indicates the special odd vertex $h_{\overline{2j-1}}$. Orange-bordered circles indicate the rearrangeable clique: $\mathcal{R}^{+}_{\overline{2j+3}} = \{h_{2j-5}, h_{2j-4}, h_{\overline{2j-3}}\}$ on the left, and $\mathcal{R}^{-}_{\overline{2j+3}} = \{h_{2j+5}, h_{2j+6}, h_{\overline{2j+7}}\}$ on the right, which is the same as those in Figure 9. The white circles indicate forbidden vertices, that cannot be connected to any of the claw leaves in $L \oplus R$.

A.2.2 Potential neighbors of claw

Here we explain the *potential neighbors* of claw, which is the neighbors of claw in $G[L \oplus R]$. Note that $G[L \oplus R]$ is a bipartite graph, and L and R are independent sets; vertices in L (or R) are not connected to each other.

The potential neighbors of claws are classified into three categories: (i) *rearrangeable clique*, (ii) *special odd vertices*, and (iii) *frozen even vertices*, which will be explained in the following.

Let the rearrangeable clique of a claw at c be denoted by $\mathcal{R}_c^\sigma = (h_c^{\mathcal{R},\sigma,1}, h_c^{\mathcal{R},\sigma,2}, h_c^{\mathcal{R},\sigma,3})$, where $\sigma \in \{+,-\}$. The three vertices in each rearrangeable clique are mutually connected, forming a clique. For claws at h_{2j-1} and $h_{\overline{2j+3}}$, the rearrangeable cliques are defined as

$$\mathcal{R}_{2j-1}^- = \mathcal{R}_{\overline{2j+3}}^+ \equiv (h_{2j-5}, h_{2j-4}, h_{\overline{2j-3}}), \quad \mathcal{R}_{2j-1}^+ = \mathcal{R}_{\overline{2j+3}}^- \equiv (h_{2j+5}, h_{2j+6}, h_{\overline{2j+7}}). \tag{96}$$

The rearrangeable clique $\mathcal{R}_c^-$ is connected to the special odd and frozen vertices of the claw at c in G, while $\mathcal{R}_c^+$ is not. These rearrangeable cliques are represented by orange-bordered circles in Figures 9–12. Note that claws at h_{2j-1} and $h_{\overline{2j+3}}$ share the same set of rearrangeable cliques, independent of the claw type. Since each rearrangeable clique forms a clique, a claw can connect to at most one vertex in each rearrangeable clique. Importantly, the possible neighbors of rearrangeable cliques connected to claws at h_{2j-1} and $h_{\overline{2j+3}}$ are also the same, independent of the claw type.

The special odd vertex for the claw at h_{2j-1} is defined as $h_{2j-1}^{\mathrm{spo}} \equiv h_{2j+3}$, and those for the claw at $h_{\overline{2j+3}}$ is defined as $h_{\overline{2j+3}}^{\mathrm{spo}} \equiv h_{\overline{2j-1}}$. These are represented by grayish-blue-bordered circles in Figures 9–12. When the leaves are connected to the special odd vertex, the claw can potentially cancel with an extended claw structure, as is explained in Figure 15.

The frozen even vertices for the claw at h_{2j-1} are defined as $h_{2j-1}^{\mathrm{frz},1} \equiv h_{2j+2}$ and $h_{2j-1}^{\mathrm{frz},2} \equiv h_{2j+4}$, and those for the claw with center $h_{\overline{2j+3}}$ are defined as $h_{\overline{2j+3}}^{\mathrm{frz},1} \equiv h_{2j}$ and $h_{\overline{2j+3}}^{\mathrm{frz},2} \equiv h_{2j-2}$. $h_c^{\mathrm{frz},2}$ is connected to $\mathcal{R}_c^+$ and $h_c^{\mathrm{frz},1}$ is not. These are represented by rectangles in Figures 9–12. When the leaves are connected to the frozen even vertices, these frozen vertices cannot be connected to any other vertices in R. This property prevents claw cancellation involving this claw, and the cancellation must then be achieved through other CC-parts or reduced to BOE-cancellation, as we will see later. Note that claws with the same center share the same set of frozen even vertices independent of the claw type.

The other neighbors are represented by white circles and are called forbidden vertices in Figures 9, 10. These are neighbors of the claw center that cannot be connected to the leaves, since R is an independent set of vertices. Also note that the claw center cannot be connected to any vertices other than the leaves; otherwise L would become a non-independent set, contradicting its definition. Thus, for example, when $L \oplus R$ contains a type A claw at h_{2j-1}, neither L nor R can include the vertices h_{2j-2} and h_{2j+2}, which are leaves of the type B claw with the same center. This leads to the rearrangeability property of claws: if $L \oplus R$ contains a claw, there exists another configuration $(L', R') \in \mathcal{S}_M^{(k)} \times \mathcal{S}_M^{(l)}$ where $L' \oplus R'$ equals $L \oplus R$ with the claw replaced by a different type of claw with the same center.

We can confirm that there are no other claws in the frustration graph G_M. The claws included in G_M are exhausted by those given above.

A.2.3 Structure of extended claws

We next introduce *extended claws*, which are subgraphs in $G[L \oplus R]$ and natural extensions of claws. The vertices in an extended claw are denoted by $\mathcal{C}_c^{n,t} = \mathcal{A}_c^n \sqcup \mathcal{B}_c^{n,t} \subset L \oplus R$ ($t \in \{A, B\}$)

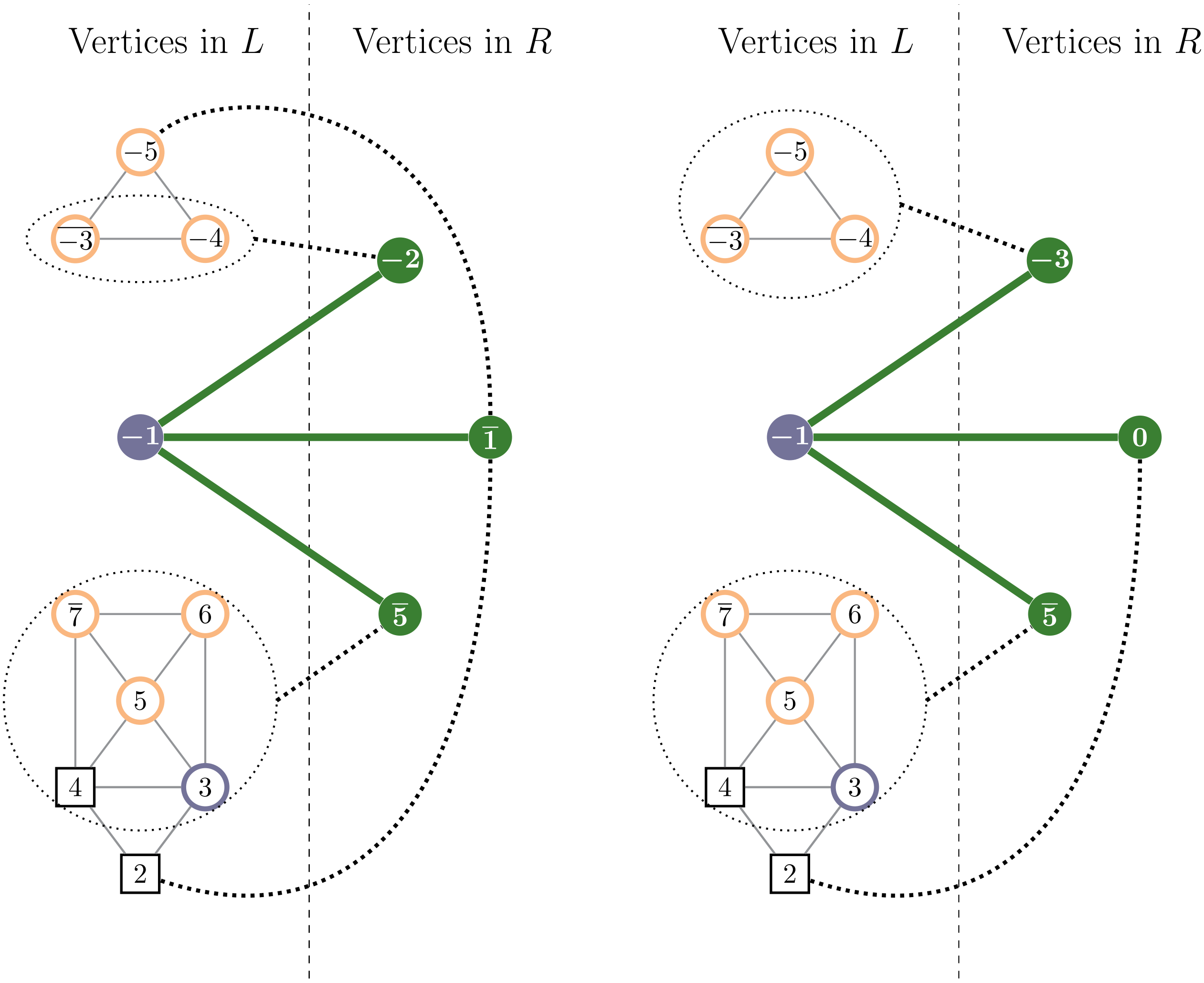

type A claw with center h_{2j-1}; type B claw with center h_{2j-1};

Figure 11: Potential neighbors of type A and type B claws in $L \oplus R$ for $(L, R) \in S_k \times S_l$. Here we assume the claw center belongs to the L side and the leaves belong to the R side; the converse case follows by a similar argument. The claw center cannot be connected to any vertices other than its three leaves. Dotted lines indicate potential edges from the leaves: a dotted line to a dotted circle means the leaf can be connected to any vertex within that dotted circle. The description of the vertex are the same as that in Figure 9.

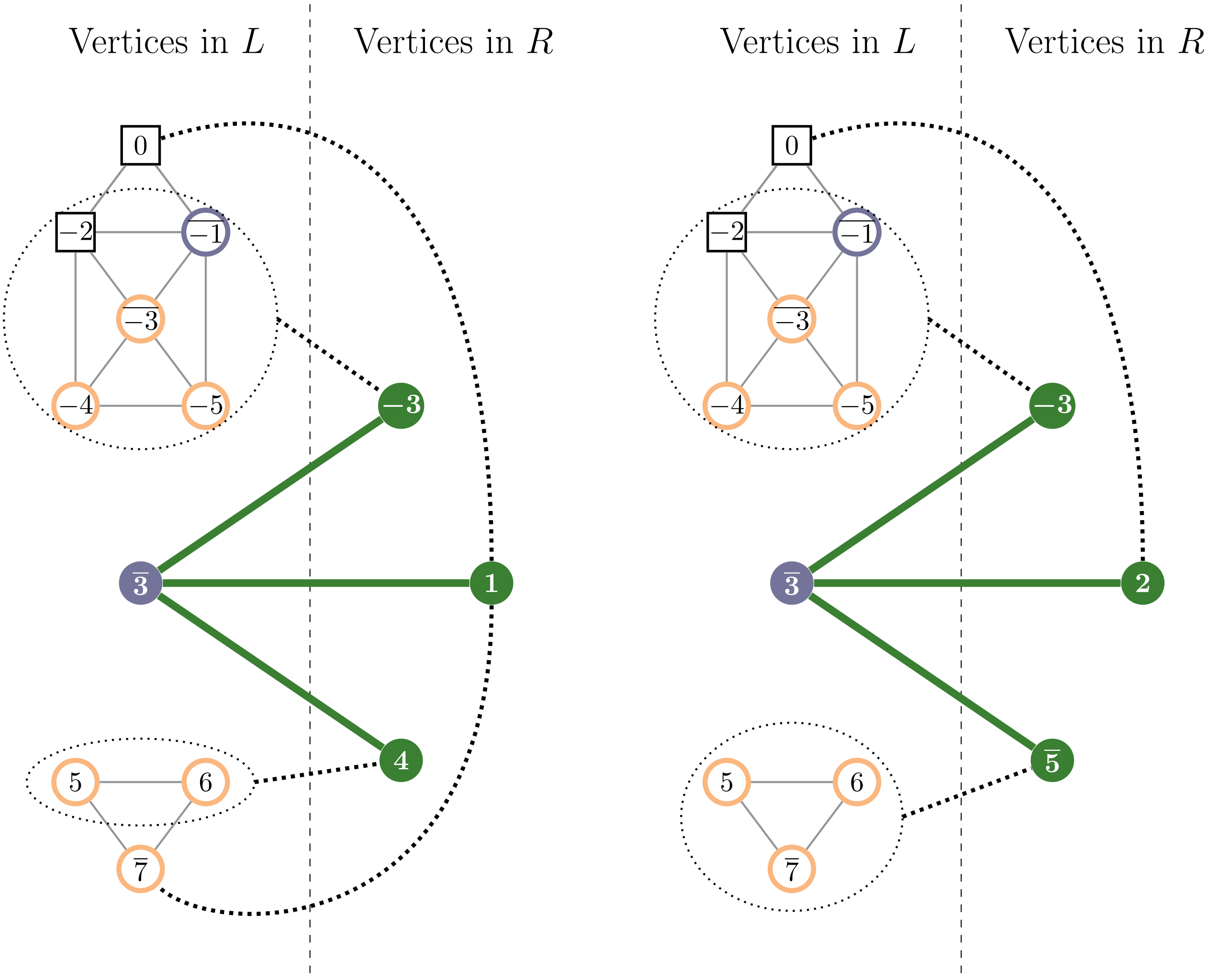

type A claw with center $h_{\overline{2j+3}}$; type B claw with center $h_{\overline{2j+3}}$;

Figure 12: Potential neighbors of type A and type B claws in $L \oplus R$ for $(L, R) \in S_k \times S_l$. Here we assume the claw center belongs to the L side and the leaves belong to the R side; the converse case follows by a similar argument. The claw center cannot be connected to any vertices other than its three leaves. Dotted lines indicate potential edges from the leaves: a dotted line to a dotted circle means the leaf can be connected to any vertex within that dotted circle. The description of the vertex are the same as that in Figure 10.

and are defined as follows:

$$\mathcal{A}_c^n = \bigsqcup_{i=1}^{n} h_{c^{(i)}}, \tag{97}$$

$$\mathcal{B}_c^{n,t} = \{h_c^{\mathcal{L},t,1}, h_c^{\mathcal{L},t,2}\} \sqcup \mathcal{B}_c^n, \quad \mathcal{B}_c^n = \bigsqcup_{i=1}^{n} h_{c^{(i)}}^{\mathcal{L}}, \tag{98}$$

where $h_{c^{(n)}}$ is recursively defined as $h_{c^{(n)}} = h_{c^{(n-1)}}^{\mathrm{spo}}$ with $h_{c^{(1)}} \equiv h_c$. Note that the leaves of the claw at h_c are included in $\mathcal{B}_c^{n,t}$: the first component of $\mathcal{B}_c^n$ is the third leaf $h_{c^{(1)}}^{\mathcal{L}} = h_c^{\mathcal{L}}$, which together with the first two vertices comprises the leaves of the claw at h_c: $\mathcal{L}_c^t = \{h_c^{\mathcal{L},t,1}, h_c^{\mathcal{L},t,2}, h_c^{\mathcal{L}}\}$. More explicitly,

$$\mathcal{A}_{2j-1}^n = \{h_{2j-1+4i}\}_{i=0}^{n-1}, \tag{99}$$

$$\mathcal{A}_{\overline{2j-1}}^n = \{h_{\overline{2j-1-4i}}\}_{i=0}^{n-1}, \tag{100}$$

$$\mathcal{B}_{2j-1}^n = \{h_{\overline{2j+5+4i}}\}_{i=0}^{n-1}, \tag{101}$$

$$\mathcal{B}_{\overline{2j-1}}^n = \{h_{2j-7-4i}\}_{i=0}^{n-1}. \tag{102}$$

Hereafter, we refer to an extended claw $\mathcal{C}_c^{n,t}$ as an "extended claw at c".

The extended claw can also be defined recursively: $\mathcal{A}_c^n = \mathcal{A}_c^{n-1} \sqcup h_{c^{(n)}}$ and $\mathcal{B}_c^n = \mathcal{B}_c^{n-1} \sqcup h_{c^{(n)}}^{\mathcal{L}}$, thus $\mathcal{C}_c^{n,t} = \mathcal{C}_c^{n-1,t} \sqcup \{h_{c^{(n)}}, h_{c^{(n)}}^{\mathcal{L}}\}$. The extended claw $\mathcal{C}_c^{n,t}$ for $n=1$ is the usual claw introduced in Section A.2.1. Note that $h_{c^{(n)}}^{\mathcal{L}}$ is the only possible neighbor of $h_{c^{(n)}}$ from $\mathcal{C}_c^{n-1,t} \sqcup \{h_{c^{(n)}}\}$ within the subgraph $L \oplus R$.

In Figure 15, we show the structure of extended claws. For extended claws at h_{2j-1} and $h_{\overline{2j+9}}$, see Figure 13 and Figure 14, respectively.

A.2.4 Potential neighbors of extended claw

We next explain the potential neighbor of the extended claw. The potential neighbors of $\mathcal{C}_c^{n,t}$ are (i) the rearrangeable clique $\mathcal{R}_c^-$, (ii) the rearrangeable clique $\mathcal{R}_{c^{(n)}}^+$, (iii) the frozen evens $\{h_{c^{(n)}}^{\mathrm{frz},1}, h_{c^{(n)}}^{\mathrm{frz},2}\}$, and (iv) the special odd $h_{c^{(n)}}^{\mathrm{spo}}$. In Figure 15, we show the possible neighbor of $\mathcal{C}_c^{n,t} \subset L \oplus R$ for $n=2$. We can see the structure of the potential neighbor of the extend claw is similar to that of the original claw.

In the following, we call the neighbor $\{h_{c^{(n)}}^{\mathrm{frz},1}, h_{c^{(n)}}^{\mathrm{frz},2}\}$ as frozen even vertices of the extended claw, and $h_{c^{(n)}}^{\mathrm{spo}}$ as the special odd of the extended claw.

The other neighbors of $\mathcal{C}_c^{n,t}$ in G is a forbidden neighbors in $L \oplus R$, which is denoted by white circles in Figure 13, 14.

A.2.5 Definition of CC-part

We give the rigorous definition of the CC-part. $\mathcal{C}_c^{n,t} \subset L \oplus R$ is called a CC-part if the neighbors of $\mathcal{C}_c^{n,t}$ in $G[L \oplus R]$ are contained in $\mathcal{R}_c^-$ or $\mathcal{R}_{c^{(n)}}^+$, if any.

We give a schematic picture of the CC-part with a claw $\mathcal{C}_c^{n=1,t}$ in Figure 16, and the CC-part with an extended claw $\mathcal{C}_c^{n=2,t}$ in Figure 17.

As we will see in Appendix A.3, when the extended claw is connected to its frozen even vertices or special odd vertex, the extended claw preserves the balance between the number of vertices from L and R in the connected component where it is included. In such cases, we can attribute the cancellation of $h_L h_R$ to other BOE components or CC-parts in $L \oplus R$ that can break this balance. The condition that $|E_{L\oplus R}|$ is odd assures the existence of such components.

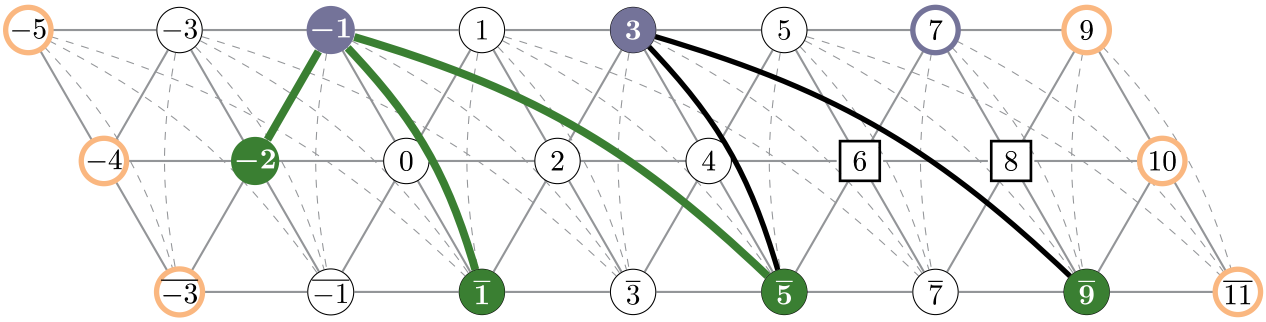

type A extended claw $\mathcal{C}^{2,A}_{2j-1}$

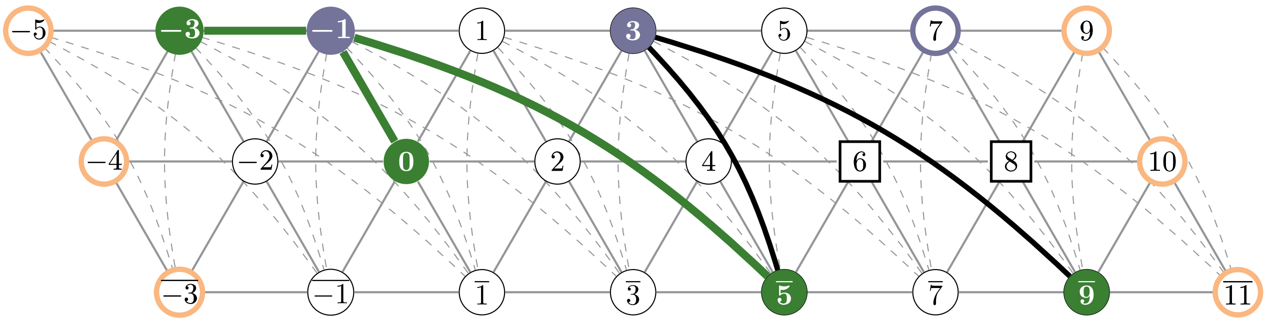

type B extended claw $\mathcal{C}^{2,B}_{2j-1}$

Figure 13: Structures of extended claws at the vertex h_{2j-1}: $\mathcal{C}^{n=2,t}_{2j-1}$. The bold green edges connect the claw center to the claw leaves, and the bold black lines represent the other edges in the extended claws, while gray edges indicate all other edges not present in the extended claws. Each vertex labeled with number i represents h_{2j+i} and labeled with $\bar{i}$ represents $h_{\overline{2j+i}}$. The grayish-blue-filled circle indicates the part $\mathcal{A}^2_{2j-1}$, and the green-filled circles indicate the part $\mathcal{B}^{2,t}_{2j-1}$ in $\mathcal{C}^{n=2,t}_{2j-1}$. Solid rectangles represent the frozen even vertices $h^{\text{frz},1}_{2j+3} = h_{2j+6}$ and $h^{\text{frz},2}_{2j+3} = h_{2j+8}$. The grayish-blue-bordered circle indicates the special odd vertex $h^{\text{spo}}_{2j+3} = h_{2j+7}$. The left orange-bordered circles constitute the rearrangeable clique $\mathcal{R}^-_{2j-1}$, and the right ones constitute $\mathcal{R}^+_{2j+3}$.

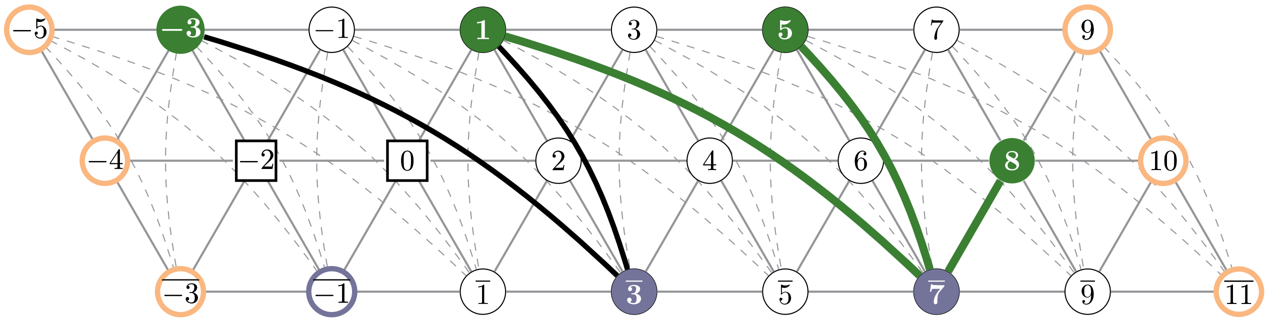

type A extended claw $\mathcal{C}^{2,A}_{\overline{2j+7}}$

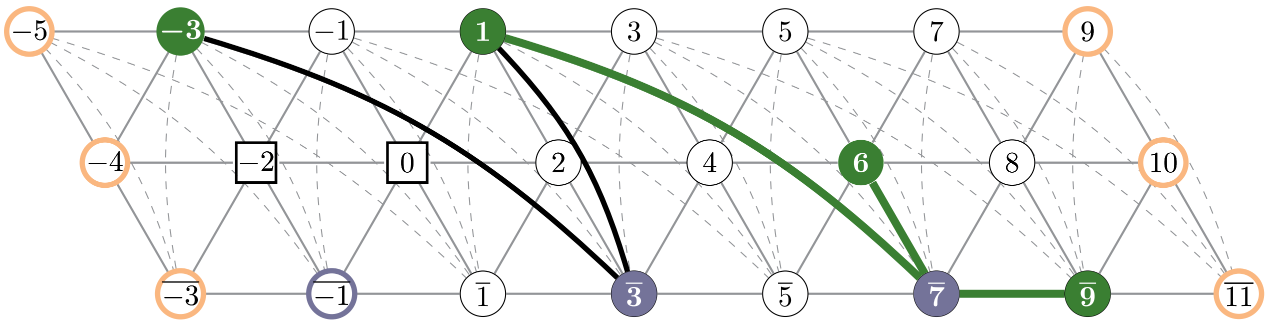

type B extended claw $\mathcal{C}^{2,B}_{\overline{2j+7}}$

Figure 14: Structures of extended claws at the vertex $h_{\overline{2j+7}}$: $\mathcal{C}^{n=2,t}_{\overline{2j+7}}$. The bold green edges connect the claw center to the claw leaves, and the bold black lines represent the other edges in the extended claws, while gray edges indicate all other edges not present in the extended claws. Each vertex labeled with number i represents h_{2j+i} and labeled with $\bar{i}$ represents $h_{\overline{2j+i}}$. The grayish-blue-filled circle indicates the part $\mathcal{A}^{2}_{\overline{2j+7}}$, and the green-filled circles indicate the part $\mathcal{B}^{2,t}_{\overline{2j+7}}$ in $\mathcal{C}^{n=2,t}_{\overline{2j+7}}$. Solid rectangles represent the frozen even vertices $h^{\text{frz},1}_{\overline{2j+3}} = h_{2j}$ and $h^{\text{frz},2}_{\overline{2j+3}} = h_{2j-2}$. The grayish-blue-bordered circle indicates the special odd vertex $h^{\text{spo}}_{\overline{2j-3}} = h_{\overline{2j-1}}$. The left orange-bordered circles constitute the rearrangeable clique $\mathcal{R}^{+}_{\overline{2j+3}}$, and the right ones constitute $\mathcal{R}^{-}_{\overline{2j+7}}$.

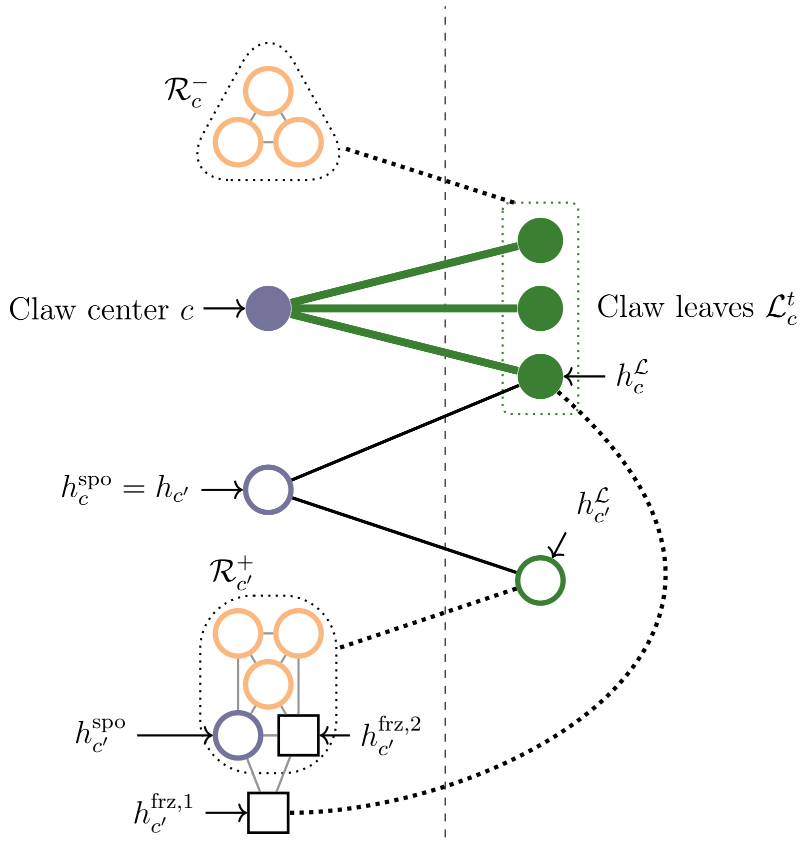

Figure 15: Potential neighbors of $\mathcal{C}_c^{n=2,t}$. The left side vertices is $\mathcal{A}_c^1 = \{h_c, h_c^{\mathrm{spo}}\}$, and the right side vertices $\mathcal{B}_c^{1,t} = \mathcal{L}_c^t \sqcup \{h_{c'}^{\mathcal{L}}\}$ where c' is determined from $h_c^{\mathrm{spo}} = h_{c'}$. The vertex $h_{c'}^{\mathcal{L}}$ is the only possible neighbor of $h_{c'}$ besides $\mathcal{L}_c^t$ in the subgraph $G[L \oplus R]$. For the definitions of the symbols (circles and dotted edges etc), see the captions of Figures 11 and 12. When an edge connects to a cluster enclosed by a dotted line, it connects to one specific vertex within that cluster; the exact connection is determined by specifying the claw center and claw type $t \in \{A, B\}$ for $\mathcal{L}_c^t$, and determined by specifying only the claw center for other dotted circles.

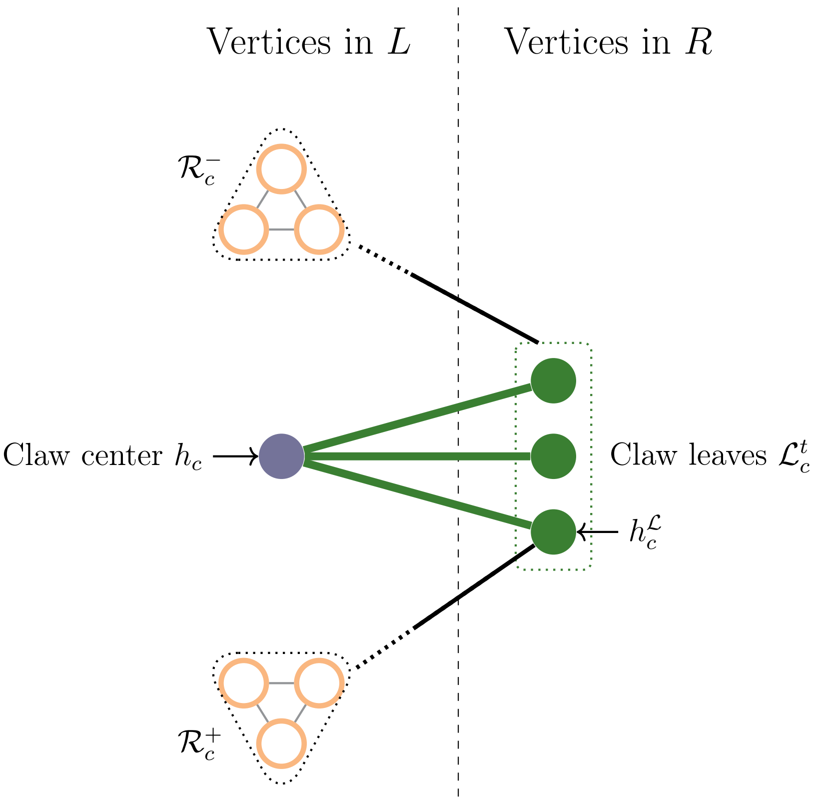

Figure 16: The simplest claw-cancellation (CC) part. The grayish-blue-filled circle in L indicates the claw center h_c. The three green-filled circles represent the claw leaves from h_c, enclosed by a green dotted triangle. The orange-bordered circles indicate the rearrangeable cliques. The solid-dotted lines from the leaves indicate two possibilities: either the leaf connects to one of the rearrangeable clique in the indicated clique, or the leaf has no connections except to its claw center. When an edge connects to a cluster enclosed by a dotted line, it connects to one specific vertex within that cluster; the exact connection is determined by specifying the claw center for $\mathcal{R}_c^{\pm}$, and determined by specifying the claw center and claw type $t \in \{A, B\}$ for $\mathcal{L}_c^t$.

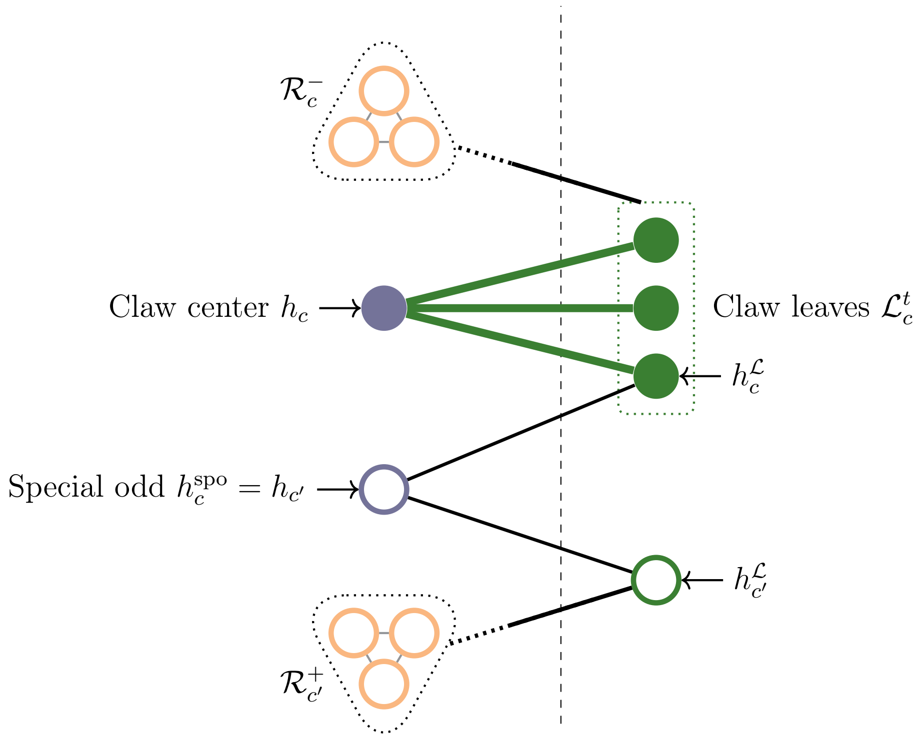

Figure 17: CC-part of extended claw $\mathcal{C}_c^{n=2,t}$. For the definitions of the symbols, please refer to Figures 16 and 15. The CC-part $\mathcal{C}_c^{n,t}$ for general n is understood similarly by extending it through the addition of vertices $\{h_{c^{(l)}}, h^{\mathcal{L}}_{c^{(l)}}\}$ where $h_{c^{(l)}} = h^{\rm spo}_{c^{(l-1)}}$ for $l = 1, \ldots, n$.

A.2.6 Cancellation via claw-cancellation part

We prove that if $L \oplus R$ includes a CC-part, then the term $h_L h_R$ in the RHS of (92) will be cancelled with other terms. We prove the cancellation for the case where the extended claw in the CC-part is $\mathcal{C}^{n,t}_{2j-1}$ in the following. The case $\mathcal{C}^{n,t}_{\overline{2j-1}}$ follows similarly due to the symmetry of the frustration graph, so we leave this case to the reader.

Consider the case where $\mathcal{C}^{n,t}_{2j-1} \subset L \oplus R$ is a CC-part and $2j-1$ is an odd integer. Then there exist four pairs $(L^{t,r}, R^{t,r}) \in \mathcal{S}^{(k)}_M \times \mathcal{S}^{(l)}_M$ for $t \in \{A, B\}$ and $r \in \{1,2\}$, with $L \oplus R \in \{L^{t,r} \oplus R^{t,r}\}_{t\in\{A,B\}, r\in\{1,2\}}$, defined by

$$
\begin{aligned}
L^{t,1} &\equiv (L \setminus \mathcal{A}^n_{2j-1}) \sqcup \mathcal{A}^n_{2j-1}, && (103)\\
R^{t,1} &\equiv (R \setminus \mathcal{B}^{n,t}_{2j-1}) \sqcup \mathcal{B}^{n,t}_{2j-1}, && (104)\\
L^{t,2} &\equiv (L \setminus \mathcal{A}^n_{2j-1}) \sqcup \mathcal{B}^{n,t}_{\overline{2j-1+4n}}, && (105)\\
R^{t,2} &\equiv (R \setminus \mathcal{B}^{n,t}_{2j-1}) \sqcup \mathcal{A}^{n}_{\overline{2j-1+4n}}. && (106)
\end{aligned}
$$

The existence of these four extended claws is assured by the fact that extended claws are connected to rearrangeable cliques if any, and are not adjacent to their special odd and frozen even vertices. For the case where the extended claw is connected to frozen even vertices or special odd vertices, see Appendix A.3.

We next show the following identity:

$$
\mathbb{A}_{2j-1}\left(\prod_{l=1}^{n} \mathbb{C}_{2j+4l-2}\right) = \left(\prod_{l=1}^{n} \mathbb{C}_{2j+4l-4}\right)\mathbb{A}_{2j-1+4n}\,, \tag{107}
$$

which can be proved recursively using the relation $\mathbb{A}_{2j-1}\mathbb{C}_{2j+2} = \mathbb{C}_{2j}\mathbb{A}_{2j+3}$ (19).

The contribution can be calculated as

$$
\begin{aligned}
&\sum_{t\in\{A,B\}}\sum_{r=1,2} h_{L^{t,r}} h_{R^{t,r}}\\
=&\sum_{t\in\{A,B\}} h_{L\setminus\mathcal{A}^n_{2j-1}}\left(h_{\mathcal{A}^n_{2j-1}} h_{\mathcal{B}^{n,t}_{2j-1}} + h_{\mathcal{B}^{n,t}_{\overline{2j-1+4n}}} h_{\mathcal{A}^n_{\overline{2j-1+4n}}}\right) h_{R\setminus\mathcal{B}^{n,t}_{2j-1}}\\
=&h_{L\setminus\mathcal{A}^n_{2j-1}}\left[\mathbb{A}_{2j-1} h_{\mathcal{A}^n_{2j-1}} h_{\mathcal{B}^n_{2j-1}} + h_{\mathcal{B}^n_{\overline{2j-1+4n}}} h_{\mathcal{A}^n_{\overline{2j-1+4n}}}\mathbb{A}_{2j-1+4n}\right] h_{R\setminus\mathcal{B}^{n,t}_{2j-1}}\\
=&(-1)^{n-1} h_{L\setminus\mathcal{A}^n_{2j-1}}\left[\mathbb{A}_{2j-1}\left(\prod_{l=1}^{n}\mathbb{C}_{2j+4l-2}\right) - \left(\prod_{l=1}^{n}\mathbb{C}_{2j+4l-4}\right)\mathbb{A}_{2j-1+4n}\right] h_{R\setminus\mathcal{B}^{n,t}_{2j-1}}\\
=&0,
\end{aligned} \tag{108}
$$

where in the second equality we have used the fact that $h_{\mathcal{B}^{n,t}_{\overline{2j-1+4n}}}$ and $h_{\mathcal{A}^n_{\overline{2j-1+4n}}}$ anticommute because the number of edges between them is odd $(2n+1)$, in the forth equality, we used the relation $h_{\mathcal{A}^n_{2j-1}} h_{\mathcal{B}^n_{2j-1}} = (-1)^{n-1}\prod_{l=1}^{n}\mathbb{C}_{2j+4l-2}$ and $h_{\mathcal{B}^n_{\overline{2j-1+4n}}} h_{\mathcal{A}^n_{\overline{2j-1+4n}}} = (-1)^n \prod_{l=1}^{n}\mathbb{C}_{2j+4l-4}$, and in the last equality we have used (107).

A.3 Exhaustiveness of cancellation mechanisms

We next prove that all cancellations in (92) can be explained by BOE components or CC-parts.

What we should consider here is the case where an extended claw in an isolated connected component $\mathcal{O} \subset L \oplus R$ is connected to its frozen even vertices or special odd vertices. Below

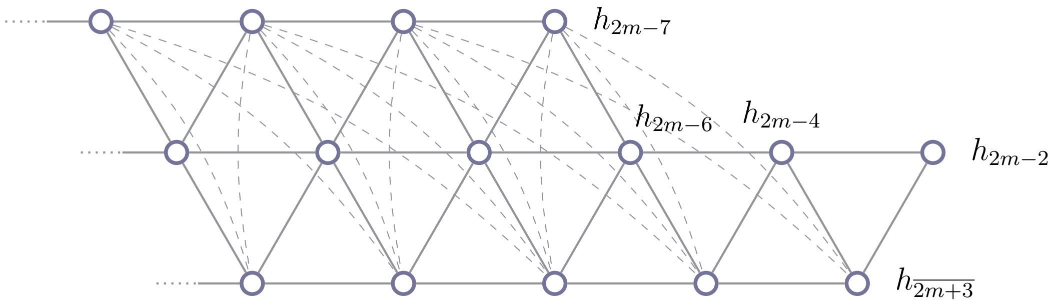

Figure 18: Free fermionic frustration graph G''_{2m-4}.

we use the notation $\mathcal{O}_L \equiv \mathcal{O} \cap L$ and $\mathcal{O}_R \equiv \mathcal{O} \cap R$. After all, such an extended claw does not have the ability to break the balance between $|\mathcal{O}_L|$ and $|\mathcal{O}_R|$. Thus, we can conclude that if an isolated connected component in $L \oplus R$ has an imbalance between $|\mathcal{O}_L|$ and $|\mathcal{O}_R|$, then $\mathcal{O}$ must contain a CC-part, which leads to cancellation. For the case where $\mathcal{O}$ has balanced $|\mathcal{O}_L|$ and $|\mathcal{O}_R|$: if $|E_{\mathcal{O}}|$ is odd, the cancellation occurs through BOE components; if $|E_{\mathcal{O}}|$ is even, we can attribute the cancellation to other isolated connected components. Note that there exists at least one isolated connected component with an odd number of edges from the fact that $|E_{L\oplus R}|$ is odd. This concludes the proof.

We next prove that an isolated connected component $\mathcal{O} \subset L \oplus R$ containing an extended claw connected to frozen even vertices or special odd vertices cannot break the balance between the number of vertices in $\mathcal{O}_L$ and $\mathcal{O}_R$.

We define an *effective vertex* $\mathcal{E}$ as a subgraph in $L \oplus R$ satisfying: (i) $|\mathcal{E} \cap L| = |\mathcal{E} \cap R| - 1$, and (ii) the possible neighbors are at most two cliques in L. The same definition applies with the roles of L and R interchanged. An effective vertex behaves as if it were a single vertex in a path. If an isolated connected component in $L \oplus R$ forms an odd path after treating all effective vertices as single vertices, the component is proven to be a BOE component and will be cancelled. We can see that an extended claw connected to its frozen even vertices or special odd vertex which is not connected to any vertex other than the leaf of the extended claw (i.e., not an extended claw in all) becomes such an effective vertex. We can see that an extended claw connected to its frozen even vertices or special odd vertex, where the special odd vertex is not connected to any vertices other than the vertex in the extended claw, becomes such an effective vertex. This concludes the proof of mutual commutativity.

B Proof of recursion for charges

In this appendix, we prove the recursions for the charges (39) and (40).

We first prove (39). We consider $G = G_{2m}$ and the clique $K = \{h_{2m}, h_{\overline{2m+1}}\}$. Using (38), we have

$$Q^{(k)}_{G_{2m}} = Q^{(k)}_{2m-1} + h_{2m} Q^{(k-1)}_{2m-3} + h_{\overline{2m+1}} Q^{(k-1)}_{G''_{2m-4}}, \tag{109}$$

where in the third term on the RHS, we define $G''_{2m-4} \equiv G_{2m} \setminus \Gamma[h_{\overline{2m+1}}]$ and use the fact that

$$G_{2m} \setminus K = G_{2m-1}, \tag{110}$$

$$G_{2m} \setminus \Gamma[h_{2m}] = G_{2m-3}. \tag{111}$$

Note that G''_{2m-4} is a free fermionic frustration graph, where we can confirm that there is no contradiction with the relation (19).

The last term on the RHS of (109) requires more careful analysis. We analyze the structure of G''_{2m-4} in Figure 18. Applying (38) with $G = G''_{2m-4}$ and $K = \{h_{2m-2}\}$, we have

$$Q^{(k-1)}_{G''_{2m-4}} = Q^{(k-1)}_{G'_{2m-4}} + h_{2m-2}Q^{(k-2)}_{2m-6}, \tag{112}$$

where we use the facts that $G''_{2m-4} \setminus \{h_{2m-2}\} = G'_{2m-4}$ and $G''_{2m-4} \setminus \Gamma[h_{2m-2}] = G_{2m-6}$.

Next, we consider the recursion (38) for $G = G_{2m-4}$ and $K = \{h_{2m-5}\}$:

$$Q^{(k-1)}_{2m-4} = Q^{(k-1)}_{G'_{2m-4}} + h_{2m-5}Q^{(k-2)}_{2m-8}, \tag{113}$$

where we use the facts that $G_{2m-4} \setminus \Gamma[h_{2m-5}] = G_{2m-8}$ and $G_{2m-4} \setminus \{h_{2m-5}\} = G'_{2m-4}$.

Combining (113) and (112), we obtain

$$Q^{(k-1)}_{G''_{2m-4}} = Q^{(k-1)}_{2m-4} + h_{2m-2}Q^{(k-2)}_{2m-6} - h_{2m-5}Q^{(k-2)}_{2m-8}. \tag{114}$$

Substituting (114) into (109), we obtain the desired recursion (39).

The proof of the charge recursion (40) follows similarly but more simply.

C Proof of recursion for polynomial

In this appendix, we prove Theorem 3: $T_G(u)T_G(-u)$ is proportional to the identity operator multiplied by the polynomial $P_G(u^2)$ (48), and derive the recursion relations for the polynomial (49) and (50).

We first introduce the notation of the transfer matrix for the pseudo-charges (37) of a general frustration graph G:

$$T_G(u) \equiv \sum_{k=0}^{\alpha_G} (-u)^k Q^{(k)}_G, \tag{115}$$

where u is the spectral parameter and α_G is the *independence number*, which is the order of the largest independent set in G. Here, an independent set is a subset of vertices with no edges between them. For $G = G_M$, the independence number is $\alpha_{G_M} = S_M$. We then introduce the following quantity for free fermionic frustration graphs G (Figure 8):

$$P_G(u^2) = T_G(u)T_G(-u)\,. \tag{116}$$

We first define some terminology regarding even holes in the frustration graph. These definitions are referred to in [8]. We denote by $\mathcal{C}^{(\text{even})}_G$ the set of all even holes in G. Two even holes C and C' are said to be *compatible* if they share no vertices and have no edges between them, i.e., if the induced subgraph $G[C \cup C']$ is disconnected with components $G[C]$ and $G[C']$. Let $\mathscr{C}^{(\text{even})}_G$ denote the collection of all subsets of $\mathcal{C}^{(\text{even})}_G$ whose elements are pairwise compatible. Each element $\mathcal{X} \in \mathscr{C}^{(\text{even})}_G$ represents a set of mutually compatible even holes. For such a subset $\mathcal{X}$, we define $\partial\mathcal{X} = \bigcup_{C\in\mathcal{X}} C$ as the union of all vertices contained in the even holes of $\mathcal{X}$. The cardinality $|\mathcal{X}|$ counts the number of even holes in $\mathcal{X}$, while $|\partial\mathcal{X}|$ denotes the total number of vertices across all holes in $\mathcal{X}$.

Consider $L, R \in \mathcal{S}_G$, and even holes $C, C' \in L \oplus R$. Here, C and C' must be compatible, because otherwise, it would contradict the definition that L and R are independent sets, which can be easily seen from the structure of the even hole in Figure 6.

From the mutual commutativity of the charges in Theorem 2, we have

$$P_G(u^2) = \sum_{\substack{s,t=0 \\ s+t=0(\bmod 2)}}^{\alpha(G)} (-1)^s u^{s+t} Q_G^{(s)} Q_G^{(t)}$$
$$= \sum_{\substack{S,T\in\mathcal{S}_G \\ |S|+|T|=0(\bmod 2)}} (-1)^{|S|} u^{|S|+|T|} (h_{S\cap T})^2 h_{S\setminus T} h_{T\setminus S} \,. \tag{117}$$

Note the following relation:

$$h_{S\setminus T} h_{T\setminus S} = (-1)^{|E_{S\oplus T}|} h_{T\setminus S} h_{S\setminus T} \,. \tag{118}$$

Then we have

$$P_G(u^2) = \sum_{\substack{S,T\in\mathcal{S}_G \\ |S|+|T|=0(\bmod 2) \\ E_{S\oplus T}=0(\bmod 2)}} (-1)^{|S|} u^{|S|+|T|} (h_{S\cap T})^2 h_{S\setminus T} h_{T\setminus S} \,. \tag{119}$$

Using the same argument as in Lemma 11 of [8] and the proof in Appendix A, we can prove

$$P_G(u^2) = \sum_{\substack{S,T\in\mathcal{S}_G \\ S\oplus T=\partial\mathcal{X} \\ \mathcal{X}\in\mathscr{C}_G^{\text{even}}}} (-x)^{|S|} h_S h_T$$
$$= \sum_{\substack{S,T\in\mathcal{S}_G \\ S\oplus T=\partial\mathcal{X} \\ \mathcal{X}\in\mathscr{C}_G^{\text{even}}}} (-u^2)^{|S|} \left(\prod_{\boldsymbol{j}\in S\cap T} b_{\boldsymbol{j}}^2\right)\left(\prod_{C\in\mathcal{X}} \mu_C\right), \tag{120}$$

where $\mu_C \equiv \mu_{2m-1}$ when the even hole is $C = C_{2m-1} \equiv \{h_{2m-3}, h_{2m}, h_{2m-2}, h_{\overline{2m+1}}\}$. Note that $\mu_{\mathcal{X}}$, which is the product of the generators in the even hole, is a scalar as explained in (14). From this, we see that $P_G(u^2)$ is a scalar polynomial in u^2. This concludes the proof of (48).

Then, we obtain the following recursion relation:

$$P_G(u^2) = P_{G\setminus K}(u^2) + \sum_{\boldsymbol{j}\in K} (-u^2) b_{\boldsymbol{j}}^2 P_{G\setminus\Gamma[\boldsymbol{j}]}(u^2) + 2 \sum_{\substack{C\in\mathcal{C}_G^{(\text{even})} \\ C\cap K\neq\emptyset}} u^4 \mu_C P_{G\setminus\Gamma[C]}(u^2) \,, \tag{121}$$

where G is a free fermionic frustration graph and K is a clique in G. The clique K must be chosen such that $G\setminus\Gamma[\boldsymbol{j}]$ for all $\boldsymbol{j}\in K$ and $G\setminus\Gamma[C]$ for all $C\in\mathcal{C}_G^{(\text{even})}$ with $C\cap K\neq\emptyset$ are free fermionic frustration graphs. We define $\Gamma[C] \equiv \bigcup_{\boldsymbol{j}\in C}\Gamma[\boldsymbol{j}]$. The factor of 2 in the third term on the r.h.s. arises from the combination of pairs (S,T) that produce the even hole C: if $S,T\in\mathcal{S}_G$ and $C\subset S\oplus T$ for some even hole C, then there exists another configuration (S',T') with $S',T'\in\mathcal{S}_G$, where $S'\equiv S\oplus C$ and $T'\equiv T\oplus C$, such that $S'\oplus T' = S\oplus T$. The factor of 2 accounts for this pair.

For $G = G_{2m-1}$ and $K = \{h_{2m-1}\}$, we can apply (121) and have

$$P_{2m-1}(u^2) = P_{2m-2}(u^2) - u^2 b_{2m-1}^2 P_{2m-4}(u^2) \,, \tag{122}$$

where we used the fact that $G_{2m-1}\setminus\Gamma(h_{2m-1}) = G_{2m-4}$. There are no even hole related terms for this case. This concludes the proof of (50).

For $G = G_{2m}$ and $K = \{h_{2m}, h_{\overline{2m+1}}\}$, we can apply (121) and have

$$P_{2m}(u^2) = P_{2m-1}(u^2) - u^2 b_{2m}^2 P_{2m-3}(u^2) - u^2 b_{\overline{2m+1}}^2 P_{G''_{2m-4}}(u^2) + 2u^4 \mu_{2m-1} P_{2m-6}(u^2)\,, \quad (123)$$

where the first to third terms can be shown in the same way as in (109), and for the last term we used $G_{2m} \setminus \Gamma[\mathcal{X}_{2m-1}] = G_{2m-6}$. In the same way as (114), we can prove the following:

$$P_{G''_{2m-4}}(u^2) = P_{2m-4}(u^2) - u^2 b_{2m-2}^2 P_{2m-6}(u^2) + u^2 b_{2m-5}^2 P_{2m-8}(u^2)\,. \quad (124)$$

Here again, there are no even hole related terms. Also note that the signs of the second and third terms are different (flipped) from those in (114).

Applying (122) to the first and second terms of (123) and substituting (124) into the third term of (123), we have

$$\begin{aligned}
P_{2m}(u^2) = &\left(P_{2m-2}(u^2) - u^2 b_{2m-1}^2 P_{2m-4}(u^2)\right) - u^2 b_{2m}^2 \left(P_{2m-4}(u^2) - u^2 b_{2m-3}^2 P_{2m-6}(u^2)\right) \\
&- u^2 b_{\overline{2m+1}}^2 \left[P_{2m-4}(u^2) - u^2 b_{2m-2}^2 P_{2m-6}(u^2) + u^2 b_{2m-5}^2 P_{2m-8}(u^2)\right] \\
&\pm 2u^4 b_{2m-3} b_{2m} b_{2m-2} b_{\overline{2m+1}} P_{2m-6}(u^2) \\
= &\, P_{2m-2}(u^2) - u^2 \left(b_{2m-1}^2 + b_{2m}^2 + b_{\overline{2m+1}}^2\right) P_{2m-4}(u^2) \\
&+ u^4 \left(b_{2m-3} b_{2m} \pm b_{2m-2} b_{\overline{2m+1}}\right)^2 P_{2m-6}(u^2) - u^4 b_{\overline{2m+1}}^2 b_{2m-5}^2 P_{2m-8}(u^2) \\
= &\, P_{2m-2}(u^2) - u^2 \mathbb{S}_{2m}^2 P_{2m-4}(u^2) + u^4 \mathbb{A}_{2m-1}^2 P_{2m-6}(u^2) - u^4 \mathbb{C}_{2m-2}^2 P_{2m-8}(u^2)\,,
\end{aligned}$$

which concludes the proof of (49).

D Proof of the independence number

In this appendix, we prove that the independence number of the frustration graph is $S_M = \lfloor (M+2)/3 \rfloor$. Note that S_M is also the degree of the polynomial $P_M(x)$ (48). For this, it is sufficient to prove that the degree of the polynomial (48) is $S_M = \lfloor (M+2)/3 \rfloor$.

From the recursions (49) and (50), we have the recursion for the degrees:

$$S_{2m} = \max(S_{2m-2}, S_{2m-4} + 1, S_{2m-6} + 2, S_{2m-8} + 2)\,, \quad (125)$$

$$S_{2m-1} = \max(S_{2m-2}, S_{2m-4} + 1)\,. \quad (126)$$

For (125), we can further simplify as

$$\begin{aligned}
S_{2m} &= \max(\max(S_{2m-2}, S_{2m-4} + 1), 1 + \max(S_{2m-4}, S_{2m-6} + 1)) \\
&= \max(S_{2m-1}, S_{2m-3} + 1)\,, \quad (127)
\end{aligned}$$

where we have used the trivial identity $S_{2m-6} \geq S_{2m-8}$ in the first equality. Thus, we have the recursion for the degree which does not depend on whether M is even or odd:

$$S_M = \max(S_{M-1}, S_{M-3} + 1)\,, \quad (128)$$

where the initial conditions are $S_1 = S_2 = S_3 = 1$.

This is the same recursion as in the original FFD case [4] . Thus, we can conclude that the independence number here is the same as that of the original FFD case: $S_M = \lfloor (M+2)/3 \rfloor$. This is the desired result.

E Proof of the free fermionic relations

Here we provide the proofs that are essential for the construction of the fermionic modes in Section 6. We only show these statements for the right-end simplicial mode that was defined in Subsection 6.2. We omit the treatment of the left-end simplicial mode in Subsection 6.3, as it is possible to arrive at the same relations after applying similar ideas akin to those presented here to the initial steps of the recursion for the transfer matrix instead. In Subsection E.1 we prove the crucial formula (63) and in Subsection E.2 the canonical anticommutation of the fermions.

E.1 The commutation relation

We would like to prove the master relation

$$T_M(u)\,(o_0 + uo_1) = (o_0 - uo_1)\,T_M(u) \tag{129}$$

where $o_0 = \chi_M,\ o_1 = \mathbb{S}_M\chi_M$ according to (71). This is equivalent to the modified inversion relation (63) after multiplying it with $T_M(-u)$ and using the inversion relation (48). As explained in Section 6 this leads to (62) in a straightforward way. After reordering, we set out to prove

$$[o_0, T_M(u)] = u\{o_1, T_M(u)\}. \tag{130}$$

We consider the odd system size $M = 2m-1$ at first. In this case $o_0 = \chi_{2m-1},\ o_1 = h_{2m-1}\chi_{2m-1}$, and using the recursion (43) and that $[\chi_{2m-1}, T_{2m-k}(u)] = 0$ for $k > 1$ we have

$$[o_0, T_{2m-1}(u)] = 2uo_1T_{2m-4}(u) \tag{131}$$

on the l.h.s. of (130). On the r.h.s. we have

$$\{o_1, T_{2m-1}(u)\} = \{o_1, T_{2m-2}(u)\} = 2o_1T_{2m-4}(u) \tag{132}$$

where we used the recursion (43) for odd system sizes and that $\{h_{2m-1}\chi_{2m-1}, h_{2m-1}\} = 0$ at first, while used the recursion (42) for even system sizes to expand $T_{2m-2}(u)$ and showed that all but the first term vanish.

To see this latter fact let us write (42) as

$$T_{2m}(u) = T_{2m-2}(u) - u\mathbb{S}_{2m}T_{2m-4}(u) + u^2\mathbb{A}_{2m-1}T_{2m-6}(u) + u^2\mathbb{C}_{2m-2}T_{2m-8}(u) \tag{133}$$

where we substituted T_{2m-1}. Then the statement boils down to showing

$$\{o_1, \mathbb{S}_{2m-2}\} = \{o_1, \mathbb{A}_{2m-3}\} = \{o_1, \mathbb{C}_{2m-4}\} = 0 \tag{134}$$

with $o_1 = h_{2m-1}\chi_{2m-1}$.

For even system sizes $M = 2m$ our task is a bit more involved. Now $o_0 = \chi_{2m}$ while $o_1 = \mathbb{S}_{2m}\chi_{2m} = (h_{2m} + h_{2m-1} + h_{\overline{2m+1}})\chi$.

At first we show that (133) simplifies to (47). The prefactors in (133) satisfy

$$[\mathbb{S}_{2m}, \mathbb{A}_{2m-1}] = \{\mathbb{S}_{2m}, \mathbb{C}_{2m-2}\} = \{\mathbb{S}_{2m}, \mathbb{A}_{2m-3}\} = \{\mathbb{S}_{2m}, \mathbb{C}_{2m-4}\} = [\mathbb{S}_{2m}, \mathbb{A}_{2m-5}] = [\mathbb{S}_{2m}, \mathbb{C}_{2m-6}] = 0\,. \tag{135}$$

Using these and their definitions in (17) and (18) the commutator and anticommutator of $T_{2m-2}(u)$ and $T_{2m-4}(u)$ with $\mathbb{S}_{2m}$ leads to

$$\{\mathbb{S}_{2m}, T_{2m-2}(u)\} = \{\mathbb{S}_{2m}, T_{2m-4}(u)\} - 2u\mathbb{A}_{2m-1}T_{2m-6}(u), \tag{136}$$

$$[\mathbb{S}_{2m}, T_{2m-4}(u)] = 2u\mathbb{C}_{2m-2}T_{2m-8}(u). \tag{137}$$

Replacing the last two terms on the r.h.s. of (133) by (136) and (137) respectively, leads to

$$T_{2m}(u) = T_{2m-2}(u) - \frac{u}{2}\{\mathbb{S}_{2m}, T_{2m-2}(u)\}, \tag{138}$$

after collecting the terms. Then, showing (131) needs commuting both sides of (47) by $[\chi_{2m}, \cdot]$. Since $[\chi_{2m}, T_{2m-k}] = 0$ for $k > 1$ one can bring this commutator inside the anticommutator on the r.h.s. of (47), giving $[\chi_{2m}, \mathbb{S}_{2m}] = -2\mathbb{S}_{2m}\chi_{2m} = -2o_1$. That is, we arrive at

$$[o_0, T_{2m}(u)] = u\{o_1, T_{2m-2}(u)\} = u\{o_1, T_{2m}(u)\}, \tag{139}$$

where it is a remaining task to prove the last equality. After applying $\{o_1, \cdot\}$ on (47) one can indeed see the cancellation of the last term on the r.h.s. as

$$\begin{aligned}\{o_1, \{\mathbb{S}_{2m}, T_{2m-2}(u)\}\} &= -\mathbb{S}_{2m}\{\mathbb{S}_{2m}, T_{2m-2}(u)\}\chi_M + \{\mathbb{S}_{2m}, T_{2m-2}(u)\}\mathbb{S}_{2m}\chi_M \\ = -\left(\mathbb{S}_{2m}^2 T_{2m-2}(u) + \mathbb{S}_{2m}T_{2m-2}(u)\mathbb{S}_{2m}\right) &+ \left(\mathbb{S}_{2m}T_{2m-2}(u)\mathbb{S}_{2m} + T_{2m-2}(u)\mathbb{S}_{2m}^2\right)\chi_M \end{aligned} \tag{140}$$

where we used to anticommute and commute χ_M through $\mathbb{S}_{2m}$ and $T_{2m-2}(u)$ respectively, and used that $\mathbb{S}_{2m}^2 \propto \mathbb{1}$.

E.2 The canonical anticommutation relations

For later convenience we introduce $\varphi_M(u) \equiv T_M(-u)\chi_M T_M(u)$. We will study the anticommutator

$$\{\varphi_M(u), \chi_M\} = \bar{T}_M(-u)T_M(u) + T_M(-u)\bar{T}_M(u) \tag{141}$$

with $\bar{T}_M(u) \equiv \chi_M T_M(u)\chi_M$, and show that it is proportional to identity. We consider the odd and even cases together. It is possible to rephrase each of the corresponding recursions (43) and (47) as

$$T_M(u) = T_{M-r_M}(u) - \frac{1}{2}[\chi_M, T_M(u)]\chi_M \tag{142}$$

$$\bar{T}_M(u) = T_{M-r_M}(u) + \frac{1}{2}[\chi_M, T_M(u)]\chi_M. \tag{143}$$

where $r_M = 1$ for M odd and $r_M = 2$ for M even. Then, after substituting (142) and (143) into (141) our anticommutator looks like

$$\begin{aligned}\{\varphi_M(u), \chi_M\} &= 2P_{M-r_M}(u^2)\mathbb{1} + \frac{1}{2}[\chi_M, T_M(-u)][\chi_M, T_M(u)] = \\ &= 2P_{M-r_M}(u^2)\mathbb{1} + \frac{1}{2}\left(\bar{T}_M(-u)T_M(u) + T_M(-u)\bar{T}_M(u) - 2P_M(u^2)\mathbb{1}\right)\end{aligned}$$

where the cross-terms dropped out from the products in (141) explicitly. Recognizing (141) and reordering leads to

$$\{\varphi_M(u), \chi_M\} = 2\left(2P_{M-r_M}(u^2) - P_M(u^2)\right)\mathbb{1}. \tag{144}$$

One can then derive the exchange relation of the fermions and the transfer matrix that reads

$$(1 - v/u_k)\,\varphi_M(u_k)T_M(v) = (1 + v/u_k)\,T_M(v)\varphi_M(u_k). \tag{145}$$

For this we have to start out as

$$\begin{aligned}\varphi_M(u_k)T_M(v) &= T_M(-u_k)o_0T_M(v)T_M(u_k) = \\ &= T_M(-u_k)\left(T_M(v)o_0 + vT_M(v)o_1 + vo_1T_M(v)\right)T_M(u_k) = \\ &= T_M(v)\varphi_M(u_k) + vu_k^{-1}T_M(v)\varphi_M(u_k) + vu_k^{-1}\varphi_M(u_k)T_M(v)\end{aligned} \tag{146}$$

where we used (129), the commutation of transfer matrices $[T_M(u), T_M(v)] = 0$ and that

$$T_M(-u_k) o_1 T_M(u_k) = \frac{1}{2}[H, \varphi_M(u_k)] = u_k^{-1} \varphi_M(u_k). \tag{147}$$

After combining (144) and (145) we arrive at

$$\begin{aligned} \{\varphi_M(u_k), \varphi_M(v)\} &= \varphi_M(u_k) T_M(-v) \chi_M T_M(v) + T_M(-v) \chi_M T_M(v) \varphi_M(u_k) \\ &= \frac{1 - v/u_k}{1 + v/u_k} T_M(-v) \{\varphi_M(u_k), \chi_M\} T_M(v) = \\ &= 4 P_{M-r_M}(u_k^2) \frac{1 - v/u_k}{1 + v/u_k} P_M(v^2) \mathbb{1}. \end{aligned} \tag{148}$$

Due to the $P_M(v^2)$ factor this expression vanishes for any $v = u_j, \quad j \neq -k$, while for $v = u_{-k} = -u_k$ one has to take the limit of the r.h.s. in (148).

$$\lim_{v \to -u_k} \{\varphi_M(u_k), \varphi_M(v)\} = 16 P_{M-r_M}(u_k^2) \prod_{j=1: j \neq k}^{S_M} \left(1 - u_k^2/u_j^2\right) \mathbb{1}. \tag{149}$$

In summary, we have

$$\Psi_k \equiv \frac{T_M(-u_k) \chi_M T_M(u_k)}{\mathcal{N}_k}, \qquad \{\Psi_k, \Psi_{k'}\} = \delta_{k+k'} \mathbb{1}, \quad k, k' \neq 0 \tag{150}$$

with normalization factors given as the square roots of the r.h.s. of (149):

$$\mathcal{N}_k = 4 \sqrt{P_{M-r_M}(u_k^2) \left(-u_k^2 P_M'(u_k^2)\right)}, \tag{151}$$

where we have rewritten the product in (149) using the derivative of the polynomial w.r.t. its argument, denoted by the prime.

When considering the anticommutator of a $\Psi_k, \ k \neq 0$ fermionic mode and the zero mode we may introduce $\mathcal{Q}_u \equiv \frac{1}{2}\left(\chi_M + \varphi_M(u)/P_M(u^2)\right)$ such that $C_0 \Psi_0 = \lim_{u \to \infty} \mathcal{Q}_u$ and using (148) and (144) it is straightforward to show that this anticommutator vanishes

$$C_0 \mathcal{N}_k \{\Psi_k, \Psi_0\} = \lim_{u \to \infty} \{\varphi_M(u_k), \mathcal{Q}_u\} = \lim_{u \to \infty} 2 P_{M-r_M}(u_k^2) \left(\frac{1}{1 + u/u_k}\right) \mathbb{1} = 0. \tag{152}$$

One can then extract the coefficients C_k from (68) for $k \neq 0$ using (144) as

$$k \neq 0: \quad \{\varphi_M(u_k), \chi_M\} = \mathcal{N}_k C_k \mathbb{1} = 4 P_{M-r_M}(u_k^2) \mathbb{1}, \tag{153}$$

leading to formula (69). We define the normalization of the zero mode through (66) such that $\Psi_0^2 = \mathbb{1}$. Since $\varphi_M^2(u) = P_M^2(u^2)\mathbb{1}$ due to the inversion formula $T_M(u) T_M(-u) = P_M(u^2)\mathbb{1}$ and the property $\chi_M^2 = \mathbb{1}$, one can also easily extract C_0 using

$$C_0^2 \mathbb{1} = \lim_{u \to \infty} \mathcal{Q}_u^2 = \lim_{u \to \infty} P_{M-r_M}(u^2)/P_M(u^2) \mathbb{1}. \tag{154}$$

Note that the limit is zero whenever the polynomial in the numerator has lower order than that in the denominator, i.e. if $S_{M-r_M} < S_M$. The completeness of the relation (68) is guaranteed by the argument using the contour integral in Appendix B of [14].

F Proof of recursion equation for the circuit

In this appendix, we give the proof for the recursion of the circuit (89). For this, we utilize the unitary local gate rather than the non-unitary local gate (84):

$$u_j(\phi_j) = \cos\frac{\phi_j}{2} + i\sin\frac{\phi_j}{2} b_j^{-1} h_j, \tag{155}$$

since the calculation is slightly simpler in this notation. The translation between these two notation is given by [13]:

$$A_j g_j(\theta_j) = u_j(\phi_j)\,, \tag{156}$$

where the relation between two angles θ_j and ϕ_j is

$$\tan\theta_j/2 = i\tan\phi_j/2\,, \tag{157}$$

and from (157) we have

$$\cos\theta_j = \frac{1}{\cos\phi_j}\,, \quad \sin\theta_j = i\frac{\sin\phi_j}{\cos\phi_j}\,. \tag{158}$$

and the scalar factor A_j is

$$A_j = \sqrt{\cos\phi_j} = \frac{1}{\sqrt{\cos\theta_j}}\,. \tag{159}$$

In the following, we use the abbreviated notations:

$$u_j \equiv u_j(\phi_j)\,, \quad u_j^- \equiv u_j(-\phi_j)\,. \tag{160}$$

We show the useful relations for the unitary local gate below:

$$u_j \hat{h}_{j+\delta} u_j = \hat{h}_{j+\delta} \quad (|\delta| = 1, 2), \tag{161}$$

$$u_j^2 = \hat{c}_j + \hat{h}_j\,, \tag{162}$$

where $\hat{h}_j \equiv i\sin\phi_j b_j^{-1} h_j$ and $\hat{c}_j \equiv \cos\phi_j$.

We define the transfer matrix for the unitary notation:

$$U_M \equiv F_M \cdot F_M^\top\,, \tag{163}$$

where F_M is defined by

$$F_{2k} = (u_2 u_1)(u_4 u_3)\cdots(u_{2k} u_{2k-1})\,, \tag{164}$$

and $F_{2k-1} \equiv F_{2k}\big|_{\phi_{2k}=0}$. The translation of $\mathcal{V}_M$ into U_M is given by

$$\mathcal{V}_M = \left(\prod_{j=1}^{M} \cos\theta_j\right) U_M\,. \tag{165}$$

We also introduce another transfer matrix as $\hat{U}_{2k} \equiv \hat{F}_{2k} \cdot \hat{F}_{2k}^\top$ where $\hat{F}_{2k} \equiv F_{2k}\big|_{\phi_{2k-1}=0}$.

In the following, we will derive the recursion relation by expanding the products in the transfer matrix U_M.

$$\begin{aligned}U_{2k} =&(u_2u_1)(u_4u_2)\cdots(u_{2k-2}u_{2k-3})(u_{2k}u_{2k-1})\cdot(u_{2k-1}u_{2k})(u_{2k-3}u_{2k-2})\cdots(u_3u_4)(u_1u_2)\\ =&\hat{c}_{2k-1}\hat{U}_{2k}+(u_2u_1)(u_4u_2)\cdots(u_{2k-2}u_{2k-3})\hat{h}_{2k-1}(u_{2k-3}u_{2k-2})\cdots(u_3u_4)(u_1u_2)\\ =&\hat{c}_{2k-1}\hat{U}_{2k}+\hat{h}_{2k-1}U_{2k-4}\,. \end{aligned}\tag{166}$$

$\hat{U}_{2k}$ can be also expanded as

$$\begin{aligned}\hat{U}_{2k} =&(u_2u_1)(u_4u_2)\cdots(u_{2k-2}u_{2k-3})u_{2k}^2(u_{2k-3}u_{2k-2})\cdots(u_3u_4)(u_1u_2)\\ =&\hat{c}_{2k}U_{2k-2}+(u_2u_1)(u_4u_2)\cdots(u_{2k-2}u_{2k-3})\hat{h}_{2k}(u_{2k-3}u_{2k-2})\cdots(u_3u_4)(u_1u_2)\\ =&\hat{c}_{2k}U_{2k-2}+(u_2u_1)(u_4u_2)\cdots(u_{2k-4}u_{2k-5})u_{2k-2}\hat{h}_{2k}(\hat{c}_{2k-3}+\hat{h}_{2k-3})\\ &\qquad\qquad\qquad\times u_{2k-2}(u_{2k-5}u_{2k-4})\cdots(u_3u_4)(u_1u_2)\\ =&\hat{c}_{2k}U_{2k-2}+(u_2u_1)(u_4u_2)\cdots(u_{2k-4}u_{2k-5})\hat{h}_{2k}(\hat{c}_{2k-3}+\hat{h}_{2k-3}u_{2k-2}^2)\\ &\qquad\qquad\qquad\times(u_{2k-5}u_{2k-4})\cdots(u_3u_4)(u_1u_2)\\ =&\hat{c}_{2k}U_{2k-2}+\hat{c}_{2k-3}\hat{h}_{2k}U_{2k-4}\\ &+\underbrace{(u_2u_1)(u_4u_2)\cdots(u_{2k-4}u_{2k-5})\hat{h}_{2k}\hat{h}_{2k-3}u_{2k-2}^2(u_{2k-5}u_{2k-4})\cdots(u_3u_4)(u_1u_2)}_{(\#1)}\,, \end{aligned}\tag{167}$$

and the last terms can further expanded as

$$\begin{aligned}(\#1) =&(u_2u_1)(u_4u_2)\cdots(u_{2k-4}u_{2k-5})\hat{h}_{2k}\hat{h}_{2k-3}(\hat{c}_{2k-2}+\hat{h}_{2k-2})(u_{2k-5}u_{2k-4})\cdots(u_1u_2)\\ =&U_{2k-6}\hat{c}_{2k-2}\hat{h}_{2k}\hat{h}_{2k-3}+\underbrace{(u_2u_1)(u_4u_2)\cdots(u_{2k-4}u_{2k-5})\hat{h}_{2k}\hat{h}_{2k-3}\hat{h}_{2k-2}(u_{2k-5}u_{2k-4})\cdots(u_1u_2)}_{(\#2)}\,, \end{aligned}\tag{168}$$

and again, the last term can be expanded as

$$\begin{aligned}(\#2) =&(u_2u_1)(u_4u_2)\cdots(u_{2k-6}u_{2k-7})(u_{2k-4}u_{2k-5})\hat{h}_{2k}\hat{h}_{2k-3}\hat{h}_{2k-2}(u_{2k-5}u_{2k-4})(u_{2k-7}u_{2k-6})\cdots(u_1u_2)\\ =&(u_2u_1)(u_4u_2)\cdots(u_{2k-6}u_{2k-7})u_{2k-4}\hat{h}_{2k}\hat{h}_{2k-3}\hat{h}_{2k-2}u_{2k-4}(u_{2k-7}u_{2k-6})\cdots(u_1u_2)\\ =&\hat{h}_{2k}\hat{h}_{2k-3}\hat{h}_{2k-2}(u_2u_1)(u_4u_2)\cdots(u_{2k-6}u_{2k-7})u_{2k-4}^2(u_{2k-7}u_{2k-6})\cdots(u_1u_2)\\ =&\hat{h}_{2k}\hat{h}_{2k-3}\hat{h}_{2k-2}\hat{U}_{2k-4}\,. \end{aligned}\tag{169}$$

Then we have

$$\hat{U}_{2k} =\hat{c}_{2k}U_{2k-2}+\hat{c}_{2k-3}\hat{h}_{2k}U_{2k-4}+\hat{h}_{2k-2}\hat{h}_{2k-3}\hat{h}_{2k}\hat{U}_{2k-4}+\hat{c}_{2k-2}\hat{h}_{2k-3}\hat{h}_{2k}U_{2k-6}\,.\tag{170}$$

Eliminating $\hat{U}_{2k}$ and $\hat{U}_{2k-4}$ from (170) using (166), we have

$$\begin{aligned}U_{2k} =&\hat{c}_{2k}\hat{c}_{2k-1}U_{2k-2}+(\hat{c}_{2k-1}\hat{c}_{2k-3}\hat{h}_{2k}+\hat{h}_{2k-1}+\frac{\hat{c}_{2k-1}}{\hat{c}_{2k-5}}\hat{h}_{2k-2}\hat{h}_{2k-3}\hat{h}_{2k})U_{2k-4}\\ &+\hat{c}_{2k-1}\hat{c}_{2k-2}\hat{h}_{2k-3}\hat{h}_{2k}U_{2k-6}+\frac{\hat{c}_{2k-1}}{\hat{c}_{2k-5}}\hat{h}_{2k-5}\hat{h}_{2k-2}\hat{h}_{2k-3}\hat{h}_{2k}U_{2k-8}\,. \end{aligned}\tag{171}$$

Using (165), we can derive the recursion for $\mathcal{V}_{2k}$:

$$\begin{aligned}\mathcal{V}_{2k} = &\left(\prod_{j=1}^{2k} c_j\right)\big[c_{2k}^{-1}c_{2k-1}^{-1}U_{2k-2} + (c_{2k-1}^{-1}c_{2k-3}^{-1}c_{2k}^{-1}h'_{2k} + c_{2k-1}^{-1}h'_{2k-1} \\ &+ c_{2k-5}c_{2k-1}^{-1}c_{2k-2}^{-1}c_{2k-3}^{-1}c_{2k}^{-1}h'_{2k-2}h'_{2k-3}h'_{2k})U_{2k-4} + c_{2k-1}^{-1}c_{2k-2}^{-1}c_{2k-3}^{-1}c_{2k}^{-1}h'_{2k-3}h'_{2k}U_{2k-6} \\ &+ c_{2k-5}c_{2k-1}^{-1}c_{2k-5}^{-1}c_{2k-2}^{-1}c_{2k-3}^{-1}c_{2k}^{-1}h'_{2k-5}h'_{2k-2}h'_{2k-3}h'_{2k}U_{2k-8}\big] \\ = &\mathcal{V}_{2k-2} + (c_{2k-2}h'_{2k} + c_{2k-3}c_{2k-2}c_{2k}h'_{2k-1} + c_{2k-5}h'_{2k-2}h'_{2k-3}h'_{2k})\mathcal{V}_{2k-4} \\ &+ c_{2k-4}c_{2k-5}h'_{2k-3}h'_{2k}\mathcal{V}_{2k-6} + c_{2k-4}c_{2k-5}c_{2k-6}c_{2k-7}h'_{2k-5}h'_{2k-2}h'_{2k-3}h'_{2k}\mathcal{V}_{2k-8}\,,\end{aligned} \tag{172}$$

where we used the following relation:

$$\hat{h}_j = \frac{1}{\cos\theta_j}h'_j\,. \tag{173}$$

We can see that the last line in (172) is the RHS of (89), thus we have proved the recursion relation (89).

By substituting $\theta_{2k} = 0$ into (172), we can also prove (90).

References

[1] P. Jordan and E. Wigner, *Über das paulische äquivalenzverbot*, Z. Physik **47**, 631 (1928), doi:10.1007/BF01331938.

[2] E. Lieb, T. Schultz and D. Mattis, *Two soluble models of an antiferromagnetic chain*, Ann. Phys. **16**(3), 407 (1961), doi:10.1016/0003-4916(61)90115-4.

[3] T. D. Schultz, D. C. Mattis and E. H. Lieb, *Two-dimensional ising model as a soluble problem of many fermions*, Rev. Mod. Phys. **36**, 856 (1964), doi:10.1103/RevModPhys.36.856.

[4] P. Fendley, *Free fermions in disguise*, J. Phys. A **52**(33), 335002 (2019), doi:10.1088/1751-8121/ab305d, 1901.08078.

[5] A. Chapman and S. T. Flammia, *Characterization of solvable spin models via graph invariants*, Quantum **4**, 278 (2020), doi:10.22331/q-2020-06-04-278, 2003.05465.

[6] M. Ogura, Y. Imamura, N. Kameyama, K. Minami and M. Sato, *Geometric criterion for solvability of lattice spin systems*, Phys. Rev. B **102**(24), 245118 (2020), doi:10.1103/PhysRevB.102.245118, 2003.13264.

[7] S. J. Elman, A. Chapman and S. T. Flammia, *Free fermions behind the disguise*, Commun. Math. Phys. **388**, 969 (2021), doi:10.1007/s00220-021-04220-w, 2012.07857.

[8] A. Chapman, S. J. Elman and R. L. Mann, *A Unified Graph-Theoretic Framework for Free-Fermion Solvability*, arXiv e-prints arXiv:2305.15625 (2023), 2305.15625.

[9] F. C. Alcaraz and R. A. Pimenta, *Free fermionic and parafermionic quantum spin chains with multispin interactions*, Phys. Rev. B **102**(12), 121101 (2020), doi:10.1103/PhysRevB.102.121101, 2005.14622.

[10] F. C. Alcaraz and R. A. Pimenta, *Integrable quantum spin chains with free fermionic and parafermionic spectrum*, Phys. Rev. B **102**, 235170 (2020), doi:10.1103/PhysRevB.102.235170, 2010.01116.

[11] R. L. Mann, S. J. Elman, D. R. Wood and A. Chapman, *A Graph-Theoretic Framework for Free-Parafermion Solvability*, arXiv e-prints (2024), 2408.09684.

[12] P. Fendley and B. Pozsgay, *Free fermions beyond Jordan and Wigner*, SciPost Physics **16**(4), 102 (2024), doi:10.21468/SciPostPhys.16.4.102, 2310.19897.

[13] K. Fukai and B. Pozsgay, *Quantum circuits with free fermions in disguise*, Journal of Physics A: Mathematical and Theoretical **58**(17), 175202 (2025), doi:10.1088/1751-8121/adcd18, 2402.02984.

[14] I. Vona, M. Mestyán and B. Pozsgay, *Exact real-time dynamics with free fermions in disguise*, Phys. Rev. B **111**(14), 144306 (2025), doi:10.1103/PhysRevB.111.144306, 2405.20832.

[15] E. Vernier and L. Piroli, *The Hilbert-space structure of free fermions in disguise*, arXiv e-prints (2025), 2507.15959.

[16] O. Makuta, B. Kuzaka and R. Augusiak, *Frustration graph formalism for qudit observables*, arXiv e-prints (2025), doi:10.48550/arXiv.2503.22400, 2503.22400.